Published online August 27, 2004

4618–4629 Nucleic Acids Research, 2004, Vol. 32, No. 15
doi:10.1093/nar/gkh766

Phosphorylation at 5′ end of guanosine stretches inhibits dimerization of G-quadruplexes and formation of a G-quadruplex interferes with the enzymatic activities of DNA enzymes

M. Khabir Uddin[1], Yoshio Kato[1], Yasuomi Takagi[1,2], Toshiyasu Mikuma[1,4] and Kazunari Taira[1,2,3,*]

[1]Gene Function Research Center and [2]iGENE Therapeutics, Inc., National Institute of Advanced Industrial Science and Technology (AIST), Central 4, 1-1-1 Higashi, Tsukuba Science City 305-8562, Japan, [3]Department of Chemistry and Biotechnology, School of Engineering, The University of Tokyo, Hongo, Tokyo 113-8656, Japan and [4]Department of Chemistry, University of Tsukuba, Tsukuba Science City 305-8571, Japan

Received February 2, 2004; Revised April 30, 2004; Accepted July 26, 2004

ABSTRACT

During an analysis of DNA enzymes by gel electrophoresis, we found that some DNA enzymes can adopt more than one conformation. The DNA enzyme Dz31 that formed more than one conformer contained a stretch of G residues. Further investigations, involving kinetic analysis and measurements of circular dichroism, indicated that this DNA enzyme and its derivatives formed G-quadruplexes. Moreover, we found that some derivative oligomers were capable of forming dimeric G-quadruplexes. We also compared the catalytic activities of Dz31 and its mutant derivatives. The present findings suggest that DNA enzymes with five or more continuous G residues are less favorable than those without G_5 in the association step in the enzymatic reaction and, thus, the choice of targets that contain a continuous stretch of C residues downstream of the cleavage site should be avoided. In addition, we found that negative charge–charge repulsion disrupted the dimerization of G-quadruplexes when a phosphate group was added directly to the 5′-terminal G of oligomers with continuous guanosine residues. In the case of 5′-phosphorylated G_5CTA, direct attachment of a phosphate group to the continuous G_5 sequence inhibited dimerization of G-quadruplexes, at least during electrophoresis on a denaturing gel.

INTRODUCTION

Unlike double-stranded DNA, single-stranded DNA can fold into well-defined, sequence-dependent tertiary structures; it can bind specifically to a variety of target molecules and it can exhibit catalytic activity similar to that of ribozymes or protein enzymes (1–3) even though no natural catalytic DNAs have been identified. DNA enzymes were discovered by *in vitro* selection procedures and were shown to catalyze chemical reactions, such as phosphoester transfer, phosphoester formation, porphyrin metalation, DNA capping and the cleavage of RNA or DNA, in the presence of divalent cations (4–10). Joyce's group and Breaker's group have developed DNA enzymes that can cleave RNAs in a sequence-specific manner and, thus, DNA enzymes may prove useful as inactivators of mRNAs of interest (11,12). The catalytic domain of a DNA enzyme is flanked by two substrate-recognition domains of seven or eight deoxyribonucleotides each, and the RNA substrate binds to the DNA enzyme through Watson–Crick base pairing (Figure 1). DNA enzymes can be complementary to ribozymes, such as hammerhead and hairpin ribozymes, and they have broad sequence-specificity and higher stability than RNA enzymes in cells. Therefore, it should be possible to utilize DNA to build new enzymes for applications both *in vitro* (13) and *in vivo* (14,15).

DNA enzymes have been engineered to act *in trans* against other RNA molecules and to catalyze the cleavage of phosphodiester bonds at specific sites to generate products with a 2′,3′-cyclic phosphate and a 5′-hydroxyl group (16). In previous studies, we showed that a DNA enzyme, designated as $DNAzyme_{(31mer)}$ or Dz3 (this DNA enzyme is referred to as Dz31 in the present paper; Figure 1) and directed against an $mRNA_{(17mer)}$ motif (b2a2), successfully cleaved its substrate at a specific position *in vivo* (14,15). The 17mer substrate designated b2a2 is a part of the *b2a2* mRNA that is transcribed from the Philadelphia chromosome, which results from reciprocal chromosomal translocations and produces cytogenetically abnormal cells in patients with chronic myelogenous leukemia (17). For our subsequent studies of structure–activity

*To whom correspondence should be addressed at Department of Chemistry and Biotechnology, School of Engineering, The University of Tokyo, Hongo, Tokyo 113-8656, Japan. Tel: +81 3 5841 8828 or +81 29 861 3015; Fax: +81 29 861 3019 or +81 3 5841 8828; Email: taira@chembio.t.u-tokyo.ac.jp
Correspondence may also be addressed to Yasuomi Takagi. Tel: +81 29 860 3203; Fax: +81 29 860 3205; Email: y-takagi@igene-therapeutics.co.jp

The authors wish it to be known that, in their opinion, the first three authors should be regarded as joint First Authors

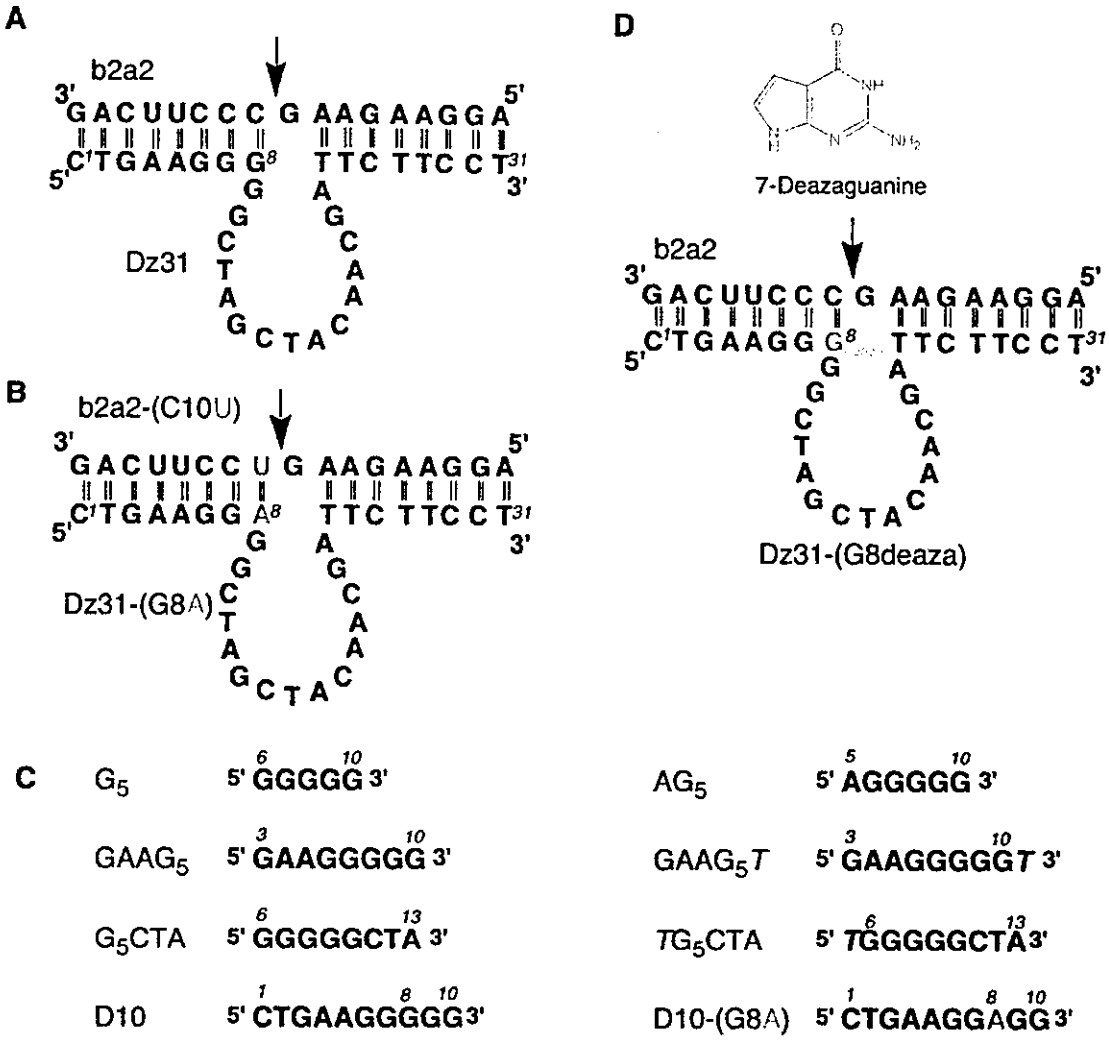

Figure 1. (A) Schematic representation of the DNA enzyme (Dz31) and its substrate (b2a2) [this enzyme was designated Dz3; (15)]. (B) The mutated DNA enzyme Dz31-(G8A) and its substrate b2a2-(C10U). (C) Segments of DNA enzymes that were examined by gel electrophoresis. (D) 7-Deazaguanine, the modified DNA enzyme Dz31-(G8deaza) and its substrate (b2a2), which were used in comparisons with wild-type Dz31.

relationships in the active core of DNA enzymes, we have focused on Dz31 and, during the present study, we found an unexpected complex, with lower mobility than expected, when we were checking the purity of Dz31 by gel electrophoresis.

In this study, we used gel electrophoresis and circular dichroism (CD) to identify the unexpected complex. We also investigated the activity of this complex in cleavage reactions. To compare the catalytic activities of Dz31, a mutated DNA enzyme$_{(31mer)}$ [Dz31-(G8A)] in which the central G within the continuous stretch of guanine nucleotides was replaced by A, and a modified DNA enzyme$_{(31mer)}$ [Dz31-(G8deaza)] in which hydrogen bonding within the stretch of G residues was disrupted, we designed substrates with an mRNA$_{(17mer)}$ motif (b2a2) and a modified mRNA$_{(17mer)}$ motif (b2a2-C10U) (Figure 1). We compared the activities of Dz31 and Dz31-(G8deaza) against the substrate with the mRNA$_{(17mer)}$ motif (b2a2) and examined the activity of Dz31-(G8A) against an mRNA$_{(17mer)}$ motif (b2a2-C10U). Dz31-(G8A), which differed from Dz31 only at the position of the eighth nucleotide (from the 5′ end) that is very important for the enzymatic reaction, was 50 times more active than Dz31 and Dz31-(G8deaza). The present findings suggest that DNA enzymes with a continuous stretch of five or more G residues participate inefficiently in the association step in the enzymatic reaction and that an adenosine at position 8 at the margin of the catalytic core of the DNA enzyme appears more suitable for effective activity than a guanine nucleotide at this position.

Guanine-rich sequences are found in biologically significant regions of the human genome, such as telomeres (18), immunoglobulin switch regions (19), gene promoter regions (20,21) and sequences associated with human diseases (22). A guanine quartet (G-quartet) is a cyclic array of four hydrogen-bonded guanine bases, in which each base is both the donor and acceptor of two hydrogen bonds with its neighbors through Hoogsteen-type base pairs. The core structure of the G-quadruplexes can be formed in many different ways, and many different structures have been observed. G-quadruplexes are known to be stable under certain conditions. In addition, G-quadruplexes are preferentially stabilized by metal ions. Monovalent ions typically interact predominantly with the negatively charged phosphate groups on DNA. However, in G-quartets, monovalent ions interact with eight carbonyl

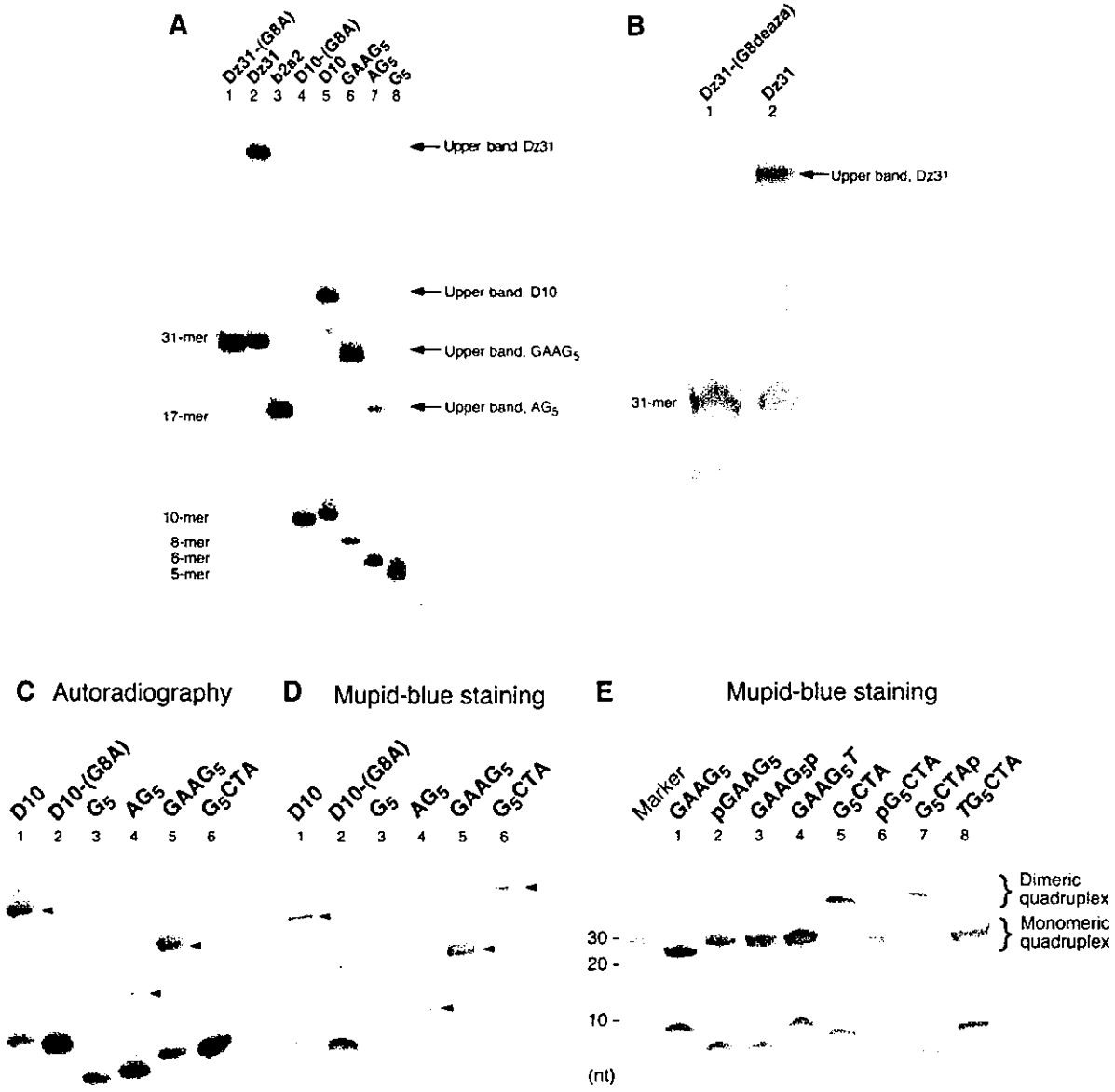

oxygen atoms. It is likely that the ion-binding properties of G-quadruplexes might be the most important contributor to their unique behavior (23).

The DNA enzyme$_{(31mer)}$ Dz31 and segments of this enzyme, namely, DNA$_{(10mer)}$ (D10), DNA$_{(8mer)}$ (GAAG$_5$) and DNA$_{(6mer)}$ (AG$_5$), which had a stretch of five continuous guanine nucleotides, each formed a band of lower mobility (upper band) during gel electrophoresis, as well as the expected band, whereas a modified DNA enzyme$_{(31mer)}$ [Dz31-(G8deaza)], a mutated DNA enzyme$_{(31mer)}$ [Dz31-(G8A)], and part of this enzyme DNA$_{(10mer)}$ [D10-(G8A)], which had no similar continuous stretch of guanine nucleotides, did not form an upper band. The measurements of CD revealed spectra typical of a G-quadruplex only in the case of oligomers with a continuous stretch of five guanine nucleotides. The CD data supported the results of gel electrophoresis and strongly suggested that the upper band on gels was due to the formation of a G-quadruplex. Importantly, some upper bands of derivative oligomers were found to be dimeric G-quadruplexes and their dimerization could be inhibited by 5′ phosphorylation.

MATERIALS AND METHODS

Synthesis and purification of substrates RNA$_{(17mer)}$ b2a2, RNA$_{(17mer)}$ b2a2-(C10U) and DNA oligomers

RNA oligonucleotides were synthesized on a DNA/RNA synthesizer (model 394; PE Applied Biosystems, Foster City, CA). The reagents for RNA synthesis were purchased from Glen Research (Sterling, VA). The crude deprotected oligonucleotides were purified on an open column and then purified on a 20% polyacrylamide gel that contained 7 M urea. Each band of interest was excised under ultraviolet irradiation, and RNA was eluted with milli-Q water (Millipore, Billerica, MA)

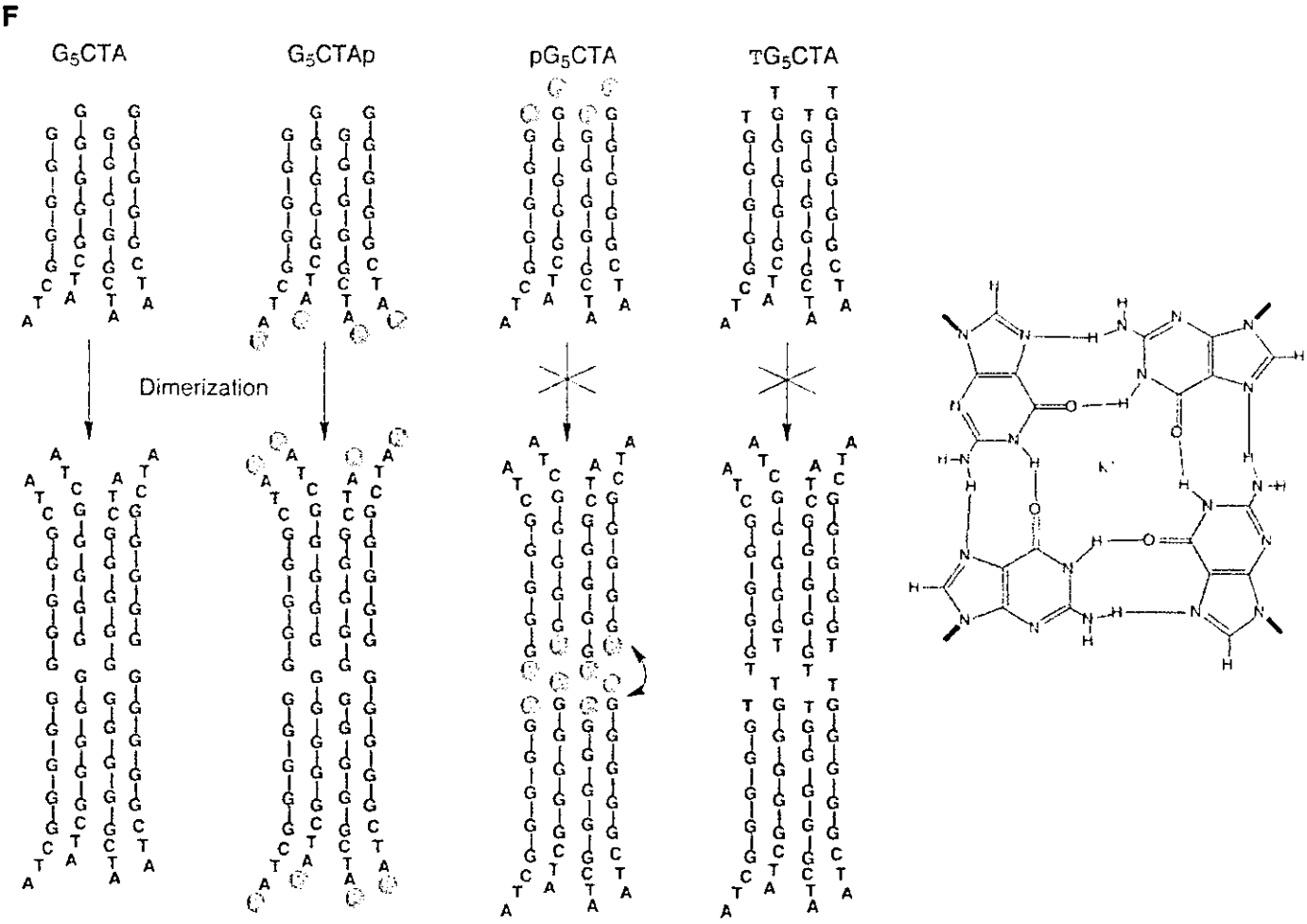

Figure 2. Gel electrophoretic analysis of the formation of G-quadruplexes. (**A–C**) 5′-^{32}P-labeled nucleotides were incubated at 4°C for 12 h in the presence of 100 mM KCl. Samples were subjected to electrophoresis on a denaturing 20% polyacrylamide gel in TBE buffer and detected by autoradiography. (**D**) The same gel used in (**C**) was stained with Mupid-Blue. Upper bands are indicated by arrowheads. (**E**) Non-labeled DNAs were subjected to electrophoresis and the gel was stained with Mupid-Blue. (**F**) Schematic representations of the effects of phosphorylation on the dimerization of a G-quadruplex. Phosphates at 5′-G terminus interfere the dimerization of G-quadruplexes.

followed by ethanol precipitation and desalted by passage through a NAP[10] column (Amersham Pharmacia Biotech AB, Uppsala, Sweden) that had been equilibrated with milli-Q water. Dz31-(G8deaza) was obtained from Japan Bio Service, Inc. (Saitama, Japan). Other DNAs were obtained from Hokkaido System Science Co., Ltd (Sapporo, Hokkaido, Japan) and Espec Oligo Service Corp. (Ibaraki, Japan). The DNAs were purified on a 20% polyacrylamide gel and preparations were desalted on a NAP[10] column.

Gel electrophoresis

Gel electrophoresis was performed with ^{32}P-labeled or non-labeled oligonucleotides. For the preparations of labeled samples, oligonucleotides were 5′ end-labeled with [γ-^{32}P]ATP using T4 polynucleotide kinase (Takara Bio, Inc., Shiga, Japan) and then mixed with unlabeled oligonucleotides to give appropriate final concentrations. Samples were analyzed on a 20% denaturing polyacrylamide gel that contained 100 mM KCl and have been equilibrated at 4°C for 3 h. Electrophoresis was performed in 100 mM Tris-borate buffer that contained 100 mM KCl overnight at room temperature. In the experiments with non-labeled oligomers, DNAs in 100 mM KCl were loaded onto 20% polyacrylamide gels without further processing, and then stained with Mupid-Blue (ADVANCE-BIO, Tokyo, Japan).

CD measurements

Samples were dissolved in 10 mM sodium cacodylate, 100 mM KCl or 1 M urea, as necessary. The pH of each solution was adjusted to 6.7. CD spectra were recorded on a spectropolarimeter (J-820; Jasco, Tokyo, Japan) equipped with a temperature controller (PTC-423L; Jasco). For each sample, scans were performed over the range of wavelengths from 220 to 350 nm and a temperature range of 5–95°C in a cell with a 1 cm path length. The scan of each respective buffer was subtracted from the scan of each sample. The spectra were plotted in units of millidegrees versus wavelength and normalized to the total concentration of each species. The cell-holding chamber was flushed with a constant stream of dry nitrogen gas to avoid condensation of water on the exterior of the cell. All the

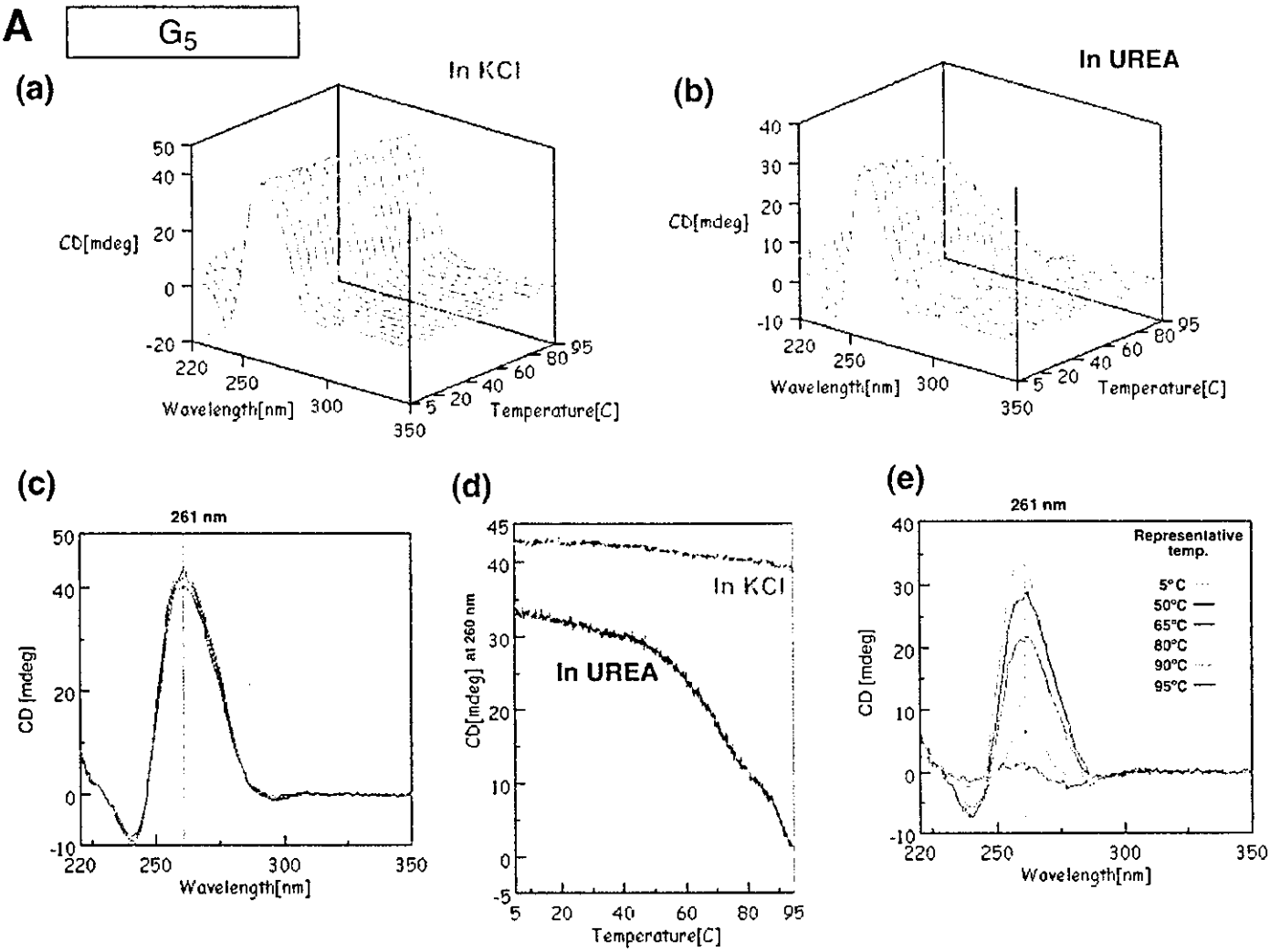

experiments were performed at least twice to confirm the reproducibility of results.

Measurements of kinetic parameters

In general, reactions were initiated by the addition of metal ions and were stopped by the removal, at appropriate intervals, of aliquots of the reaction mixture, which were mixed with an equivalent volume of a solution that contained 100 mM EDTA, 9 M urea, 0.1% xylene cyanol and 0.1% bromophenol blue. The substrates were labeled with [γ-^{32}P]ATP by T4 polynucleotide kinase. Substrates and 5′-cleaved products were separated by electrophoresis on a 20% polyacrylamide/7 M urea denaturing gel and were detected by autoradiography. The extent of cleavage was determined by quantitation of radioactivity in the bands of substrate and product with a Bio-Image Analyzer (STORM; Molecular Dynamics, Sunnyvale, CA).

Assays of activities of Dz31 and Dz31-(G8deaza) were performed in 25 mM $MgCl_2$ and 50 mM Tris–HCl (pH 8.0) at 37°C, under single-turnover conditions, with incubations for 20, 40, 60, 120, 240 and 420 min. In the case of Dz31-(G8A), 50 mM Bis-Tris–HCl (pH 6.0) buffer was used and reaction mixtures were incubated for 5, 10, 20, 30, 60 and 120 min. To obtain kinetic parameters, we performed reactions under multiple-turnover conditions using 0.05–10 μM DNA enzyme, 1–200 μM RNA, 25 mM $MgCl_2$ and 50 mM Tris–HCl buffer (pH 8.0) at 37°C. Values of K_m and k_{cat} were calculated from Eadie–Hofstee plots.

RESULTS AND DISCUSSION

Formation and identification of a low-mobility form of DNA enzyme

We examined the formation of low-mobility forms (upper bands) of DNA enzymes and of segments of these enzymes by non-denaturing and denaturing PAGE (Figure 2). Figure 1 shows the sequences of DNA enzymes and the segments of these enzymes that we used in these experiments and their corresponding mobilities on a denaturing polyacrylamide gel are shown in Figure 2A and B. The mutant DNA enzyme Dz31-(G8A) (Figure 1B) and the modified DNA enzyme Dz31-(G8deaza) (Figure 1D) differed from the parental Dz31 (Figure 1A) in that the continuous stretch of five G residues was disrupted. In the experiments for which results are shown in Figure 2A and B, the oligonucleotides were denatured completely by heating at 96°C for 3 min, then they were allowed to equilibrate at the desired temperature

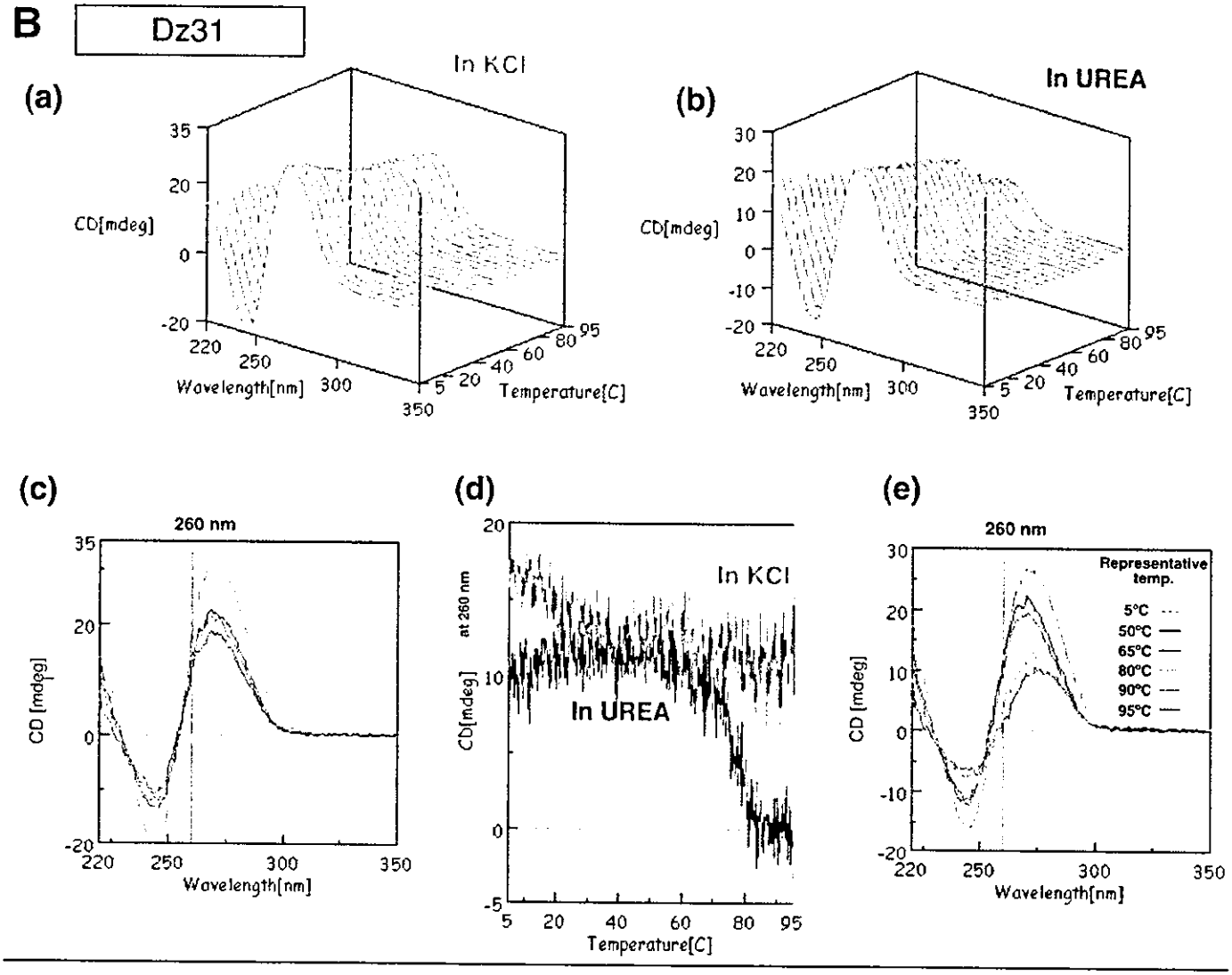

for 4 h in the presence of K^+ ions before being loaded onto 20% non-denaturing and denaturing polyacrylamide gels that were maintained at a specific temperature during electrophoresis. The samples were initially radiolabeled at their 5′ termini with [γ-^{32}P]ATP and purified by gel electrophoresis. Then, unlabeled oligonucleotides were mixed with labeled oligonucleotides to give the appropriate concentrations.

Dz31 and its derivatives, D10, $GAAG_5$ and AG_5, each yielded two bands during electrophoresis on a 20% non-denaturing gel in the absence of urea (data not shown). They also yielded two bands on a denaturing polyacrylamide gel in the presence of urea (Figure 2A). In contrast, Dz31-(G8A) and its derivative D10-(G8A) each yielded a single band (Figure 2A, lanes 1 and 4), as did Dz31-(G8deaza), on a denaturing gel (Figure 2B, lane 1). The mobilities of the lower bands indicated that the free oligonucleotides were of the expected size relative to that of the marker. The mobility of the upper band suggested that it was composed of material of 4 times the molecular weight of the material in the lower band. In other words, the mobility of a reference oligonucleotide with 4 times the molecular weight of Dz31 was almost the same as that of the material in the upper band (data not shown). According to the literature (23–25), our data suggested that the material in the upper band might have been a tetramer formed by intermolecular hydrogen bonding (Figure 2F).

To examine this hypothesis, we mutated to yield Dz31-(G8A) and its derivative D10-(G8A) at G8, the middle guanine nucleotide in the continuous stretch of five guanosine, changing G to A. In Dz31-(G8deaza) (Figure 1D), this G residue was modified by 7-deazaguanine, which breaks the hydrogen bond between the imidazole nitrogen (N^7) and the exocyclic-amine group of another guanine nucleotide. This mutation prevented the appearance of an upper band (Figure 2B). Therefore, it appeared that the upper bands were due to the five adjacent guanine nucleotides in the sequences, which should easily form a G-quadruplex as a result of intermolecular aggregation (23–28). Thawing and melting increased the intensity of the upper band of both Dz31 and its derivatives (data not shown), in agreement with previously reported results (29).

Interference with dimerization of G-quadruplexes by terminal phosphate groups

To enhance our understanding of the formation of G-quadruplexes, we also examined several oligonucleotides

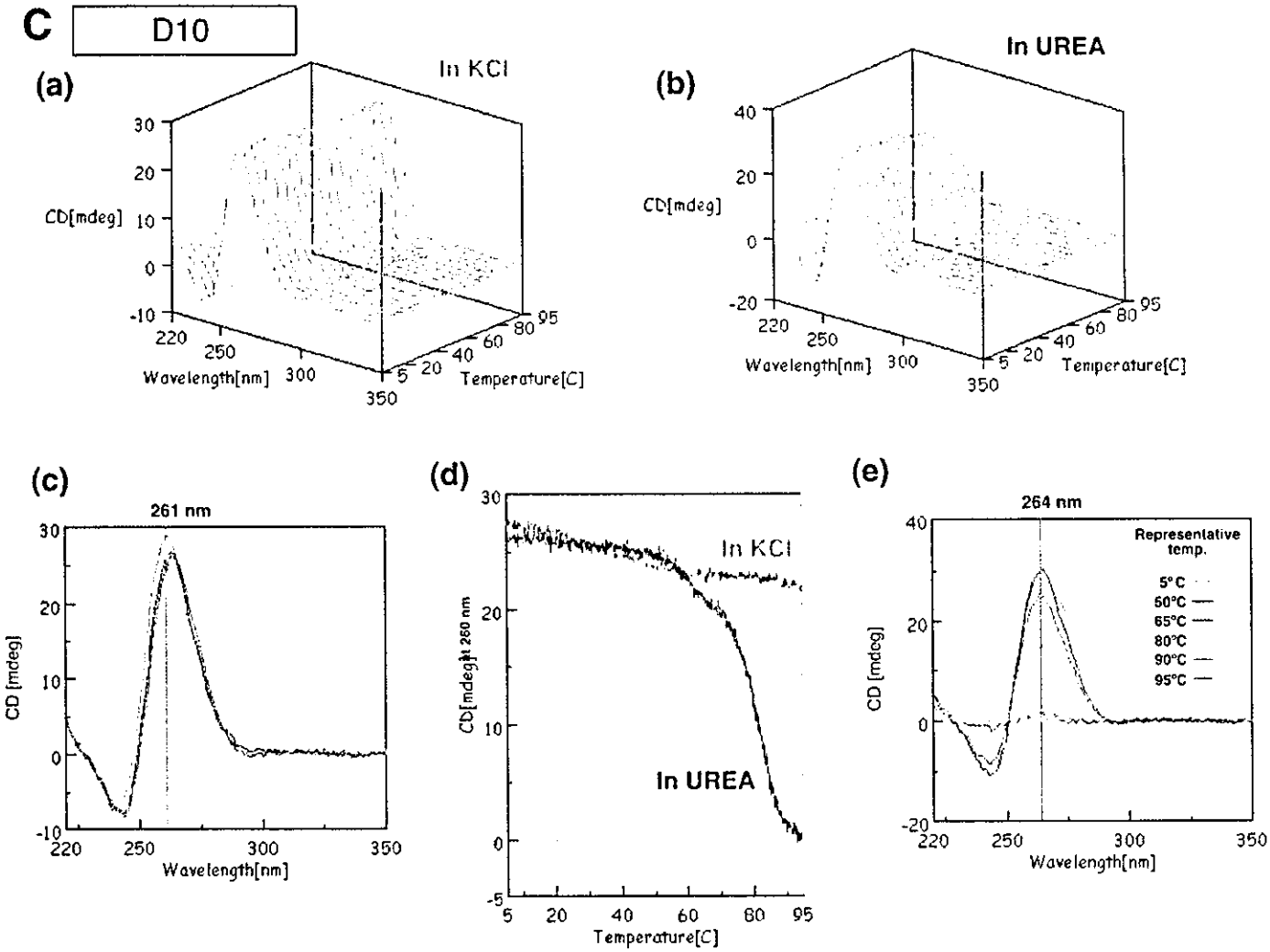

whose sequences were derived from Dz31. For the preparation of the phosphorylated oligomers shown in Figure 2C, we used T4 polynucleotide kinase to label oligomers with [γ-^{32}P]ATP. As shown in Figure 2C, $GAAG_5$ formed an upper band, but G_5CTA and G_5 did not. It is probable that negative charge–charge repulsion disrupted the formation of a G-quadruplex when a phosphate group was added directly to the 5′-terminal G of a stretch of four or more guanosine residues. In fact, Figure 2C shows that no upper bands were formed by G_5CTA and G_5, which might have a phosphate group at the 5′-terminal end of the G_5 region.

In the experiments for which results are shown in Figure 2D, we used the new reagent Mupid-Blue for the high-sensitivity detection of non-labeled oligomers. In contrast to the apparent absence of a G-quadruplex in Figure 2C, staining with Mupid-Blue indicated that $GAAG_5$ and G_5CTA yielded upper bands in each case, probably a result of the formation of a parallel G-quadruplex (Figure 2D, lanes 5 and 6). Therefore, the absence of upper bands that corresponded to G_5CTA and G_5 in Figure 2C was due to the fact that the T4 polynucleotide kinase was unable to attach phosphate groups to the termini of the G-quadruplexes and it was not due to disruption of the formation of a G-quadruplex by negative charge–charge repulsion.

To analyze the effect of phosphate groups, we prepared several oligomers with and without a phosphate group. The phosphorylated oligomers used in experiments for which results are shown in Figure 2E were synthesized by chemical addition of a phosphate group at the 5′ or 3′ end. As shown in Figure 2E, upper bands were detected in cases of $GAAG_5$ (lanes 1–3) and G_5CTA (lanes 5–7) with or without a terminal phosphate.

Although the formation of these G-quadruplexes was very reasonable with 'G-continuous' DNAs, we did note an unexpectedly large difference in terms of electrophoretic mobility between G_5CTA and pG_5CTA (Figure 2E, lanes 5 and 6). We postulated that the G-quadruplexes formed by four molecules of G_5CTA might form a dimeric G-quadruplex (two molecules of G-quadruplexes), as shown in Figure 2F. Since this kind of head-to-head dimerization of two sets of G-quadruplexes is known to be inhibited by the addition of one thymine nucleotide at the 5′ terminus (30–32) and in an attempt to explain the difference in mobilities, we prepared a one-thymine-nucleotide-supplemented oligomer (TG_5CTA)

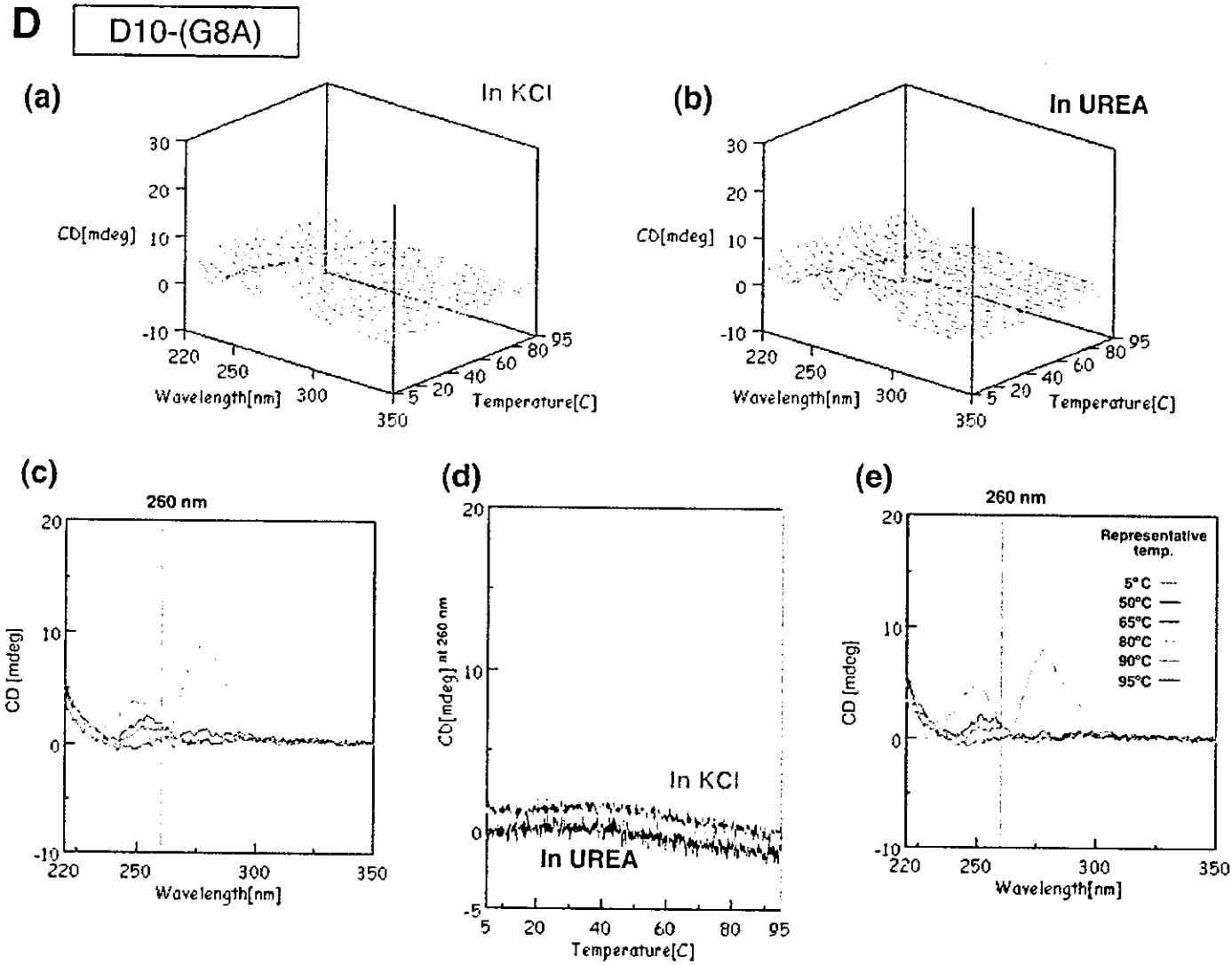

Figure 3. CD spectra of G_5 (**A**), Dz31 (**B**), D10 (**C**) and D10-(G8A) (**D**). Changes in spectra in KCl (a) and in urea (b) upon changes in temperature are shown. (c) The spectra in KCl are shown in two-dimensional graphs of CD (mdeg) versus wavelength (nm) at representative temperatures of 5, 50, 65, 80, 90 and 95°C. The vertical line exhibits the indicated wavelength, 260 or 261 nm. (d) Comparison of peak heights (mdeg) at 260 nm upon changes in temperature in KCl and in urea. (e) The spectra in urea as two-dimensional graphs of peak height (mdeg) versus wavelength (nm) at representative temperatures of 5, 50, 65, 80, 90 and 95°C. The vertical line exhibits the indicated wavelength, 260 or 261 nm.

and subjected it to gel electrophoretic analysis. We found that the mobility of TG$_5$CTA was almost identical to that of pG$_5$CTA, a monomeric G-quadruplex (Figure 2E). It appears that both TG$_5$CTA and pG$_5$CTA formed a simple parallel G-quadruplex.

While the reasons for these interesting phenomena are now somewhat clearer, several questions remain. The mobility of GAAG$_5$, which is potentially capable of forming a tail-to-tail dimeric G-quadruplex, was nearly the same as that of the monomeric G-quadruplex of GAAG$_5T$ (Figure 2E, lanes 1 and 4). It appears that GAAG$_5$ formed a simple parallel G-quadruplex in the same way as did GAAG$_5T$, despite the fact that most of the corresponding oligonucleotides examined in earlier similar studies formed a dimeric G-quadruplex with a 3′-G terminus (30–32). We are at present trying to examine this issue by analyzing many related derivatives.

Finally, although the newly discovered dimerization of the G-quadruplexes formed by G$_5$CTA is not unexpected, considering the G–G face interactions, it is noteworthy that the addition of a phosphate group at the 'G-terminal' end (pG$_5$CTA) interfered with the dimerization of G-quadruplexes, just as the addition of a thymidine disrupted the formation of dimers (Figure 2E and F). To our knowledge, this is the first demonstration of interference in the G–G face interactions by terminal phosphate groups.

CD spectra of various oligomers

As noted above, the unexpected upper bands seen after gel electrophoresis seemed to be due to the formation of monomeric and dimeric G-quadruplexes. A simple way to confirm such a possibility is to record the CD spectra of such oligomers since a four-stranded quadruplex has a very specific spectrum that is due to the formation of a G-quadruplex. For example, parallel four-stranded quadruplexes are known to have a characteristic strong positive CD band at ~262 nm and a

negative band at 240 nm, whereas antiparallel folded quadruplexes have a positive band at 295 nm and a negative band at 260 nm (25). We applied this technique to the oligomers used in this study and confirmed that G_5 yielded spectral pattern of a parallel four-stranded quadruplex, as a positive control. As shown in Figure 3A(a), the spectra that we recorded coincided with those in previous reports by other groups, with a characteristic strong positive CD peak at 260–263 nm and a negative peak at 240 nm in the presence of 100 mM of KCl, at neutral pH, over a wide range of temperatures. In the presence of 1 M urea and ~10 mM NaCl (a component of the buffered solution) instead of 100 mM KCl, these strong peaks disappeared at higher temperatures, as shown in Figure 3A(b). This phenomenon was not unexpected since urea breaks hydrogen bonds between base pairs by interacting with functional groups of nucleobases. We defined the spectra and the changes in spectra with changes in temperature in the presence of 100 mM KCl or 1 M urea without K^+ ions as the criteria by which the presence or absence of a four-stranded quadruplex is assessed.

We monitored the CD spectra of Dz31 with changes in temperature in the presence of 100 mM KCl and in 1 M urea without K^+ ions. As shown in Figure 3B, strong positive and negative peaks were observed above 270 nm and above 240 nm, respectively, over the entire range of temperatures examined. These peaks did not disappear, even at 95°C and in the presence of 1 M urea. However, the value at 260 nm decreased dramatically, falling to zero in the case of urea, with a smaller decrease in the case of KCl, as shown in Figure 3B(c–e). Although the spectral patterns of Dz31 upon changes in temperature were somewhat ambiguous, the difference between the changes in intensities at 260 nm suggests the existence of a four-stranded quadruplex in the presence of KCl. The ambiguity might have been due to the existence of several other spectral forms, e.g. the catalytic core.

To facilitate our analysis, we decided to monitor the spectra of D10 at various temperatures. The sequence of the D10 motif is the same as that of the first 10 nt from the 5′ end of Dz31. The spectrum had strong positive and negative peaks at 261 and 240 nm respectively, as seen also in the spectrum of G_5 (Figure 3C). Thus, the region adjacent to the continuous stretch of five guanosine nucleotides in D10 did not affect the formation of parallel four-stranded quadruplexes in KCl. In the presence of 1 M urea without KCl, the heights of peaks at 264 and 240 nm fell to zero at higher temperatures, as seen also in the case of G_5 itself [Figure 3C(c–e)].

Comparison of the results of CD spectroscopy and gel electrophoresis

As noted in our discussion of the results of gel electrophoresis, several oligomers containing five adjacent guanosine nucleotides, such as Dz31, D10, $GAAG_5$ and AG_5, yielded unexpected bands with reduced mobility, as well as the expected bands, during electrophoresis, namely, 'upper bands' (Figure 2A). These oligomers yielded similar CD spectral patterns and changes in patterns in KCl and urea, even though the spectra of Dz31 were rather complicated. Since the patterns of CD spectra were due, apparently, to parallel four-stranded quadruplexes that were associated with the formation of G-quadruplexes, it seems likely that the upper bands were due to the complexes that consisted of parallel four-stranded quadruplexes.

In contrast to the above-described results, D10-(G8A) did not form an upper band on the gel (Figure 2A) and did not yield a CD spectrum typical of a parallel four-stranded quadruplex (Figure 3D). This result was to be expected since D10-(G8A) did not include five adjacent guanosine nucleotides: the middle guanosine was replaced by adenosine and the formation of a G-quadruplex was inhibited. Comparing the CD spectra and results of electrophoresis for Dz31 and D10 with those for Dz31-(G8A) and D10-(G8A), we can clearly see that four or more adjacent guanosine nucleotides are responsible for the formation of a G-quadruplex by the DNA enzyme.

Interference in reactions by the G-quadruplex

The sequences of the DNA enzymes and the substrates that bind through Watson–Crick base pairing are shown in Figure 1. We found earlier that Dz31, which is 31 nt long, was the most effective DNA enzyme; it cleaved the substrate between the indicated guanosine and cytidine residues of *b2a2* mRNA (14,15). To investigate the influence of the G-quadruplex on catalysis by the DNA enzyme, we prepared two analogs, Dz31-(G8A) and Dz31-(G8deaza). Dz31-(G8A) included adenosine instead of guanosine at position 8 in Dz31. The replacement of G by A in the middle of the five adjacent guanosine residues hinders the formation of a parallel four-stranded quadruplex. Dz31-(G8deaza) had an N^7-deaza-guanosine moiety at position 8 and it too failed to yield an upper band on gels (Figure 2B). D10-(G8A) also did not produce CD patterns characteristic of the formation of a G-quadruplex (Figure 3D). We adjusted the substrate of Dz31-(G8A), by changing C to U, to allow the formation

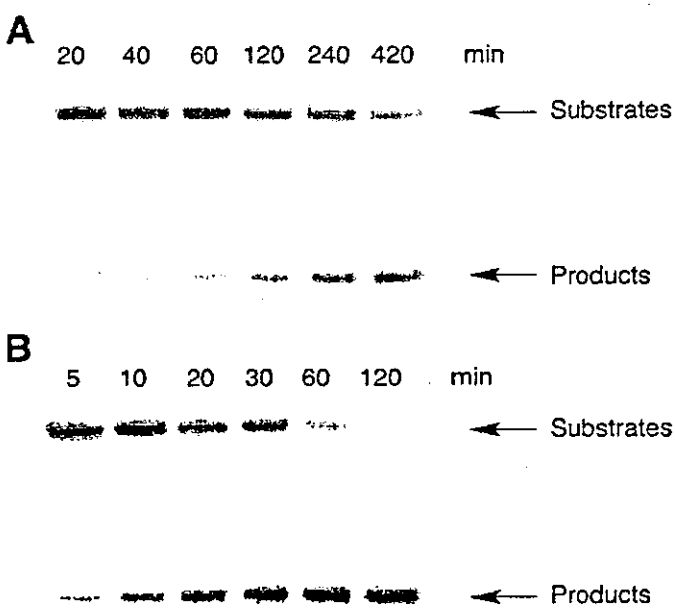

Figure 4. Autoradiograms showing the products of reactions in the presence of 25 mM Mg^{2+} at 37°C: (**A**) 50 mM Tris (pH 8.0) with catalysis by Dz31; (**B**) 50 mM Bis-Tris (pH 6.0) with catalysis by Dz31-(G8A).

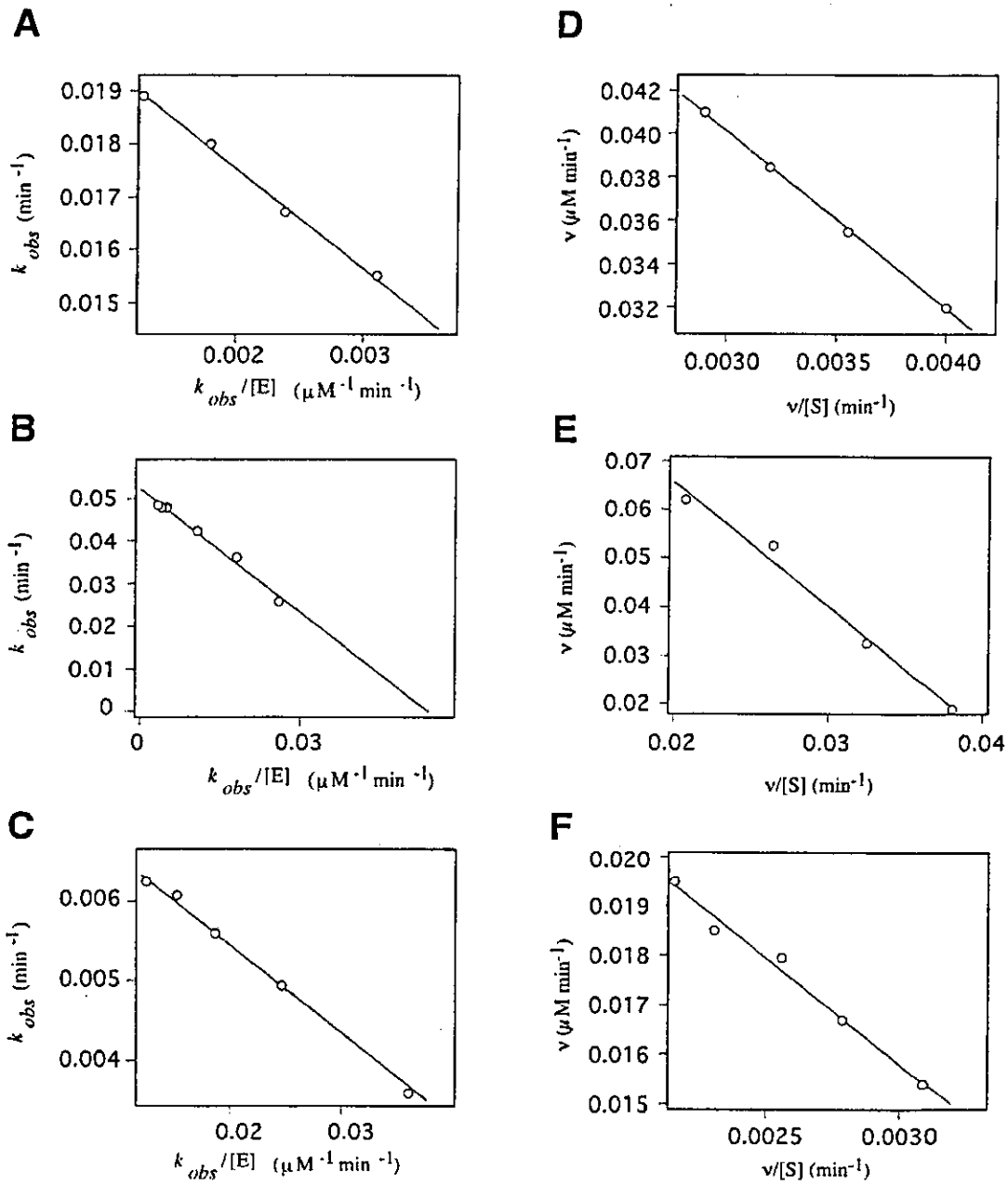

Figure 5. Determination of kinetic parameters from the equation $k_{obs} = k_{cleav} - (k_{obs} \times K_d)/[E]$ (A–C) and Eadie–Hofstee plots (D–F). Reactions were performed in the presence of 25 mM Mg^{2+} at 37°C, under single-turnover conditions (A–C) and in the presence of 25 mM Mg^{2+} in 50 mM Tris (pH 8.0), at 37°C under multiple-turnover conditions (D–F). (A) Kinetic data for Dz31 were obtained from reactions in 50 mM of Tris (pH 8.0) and yielded a K_m of 1.89 μM and a k_{cat} of 0.02 min^{-1}. (B) Values of K_m of 0.96 μM and of k_{cat} of 0.05 min^{-1} were obtained for Dz31-(G8A) from reactions in 50 mM of Bis-Tris (pH 6.0). (C) Kinetic data for Dz31-(G8deaza) were obtained from reactions in 50 mM Tris (pH 8.0) and yielded a K_m of 0.11 μM and a k_{cat} of 0.016 min^{-1}. (D) Data for Dz31 yielded a K_m of 8.2 μM and a k_{cat} of 0.05 min^{-1}. (E) Data for Dz31-(G8A) yielded a K_m of 2.93 μM and a k_{cat} of 2.35 min^{-1}. (F) Data for Dz31-(G8deaza) yielded a K_m of 4.3 μM and a k_{cat} of 0.10 min^{-1}.

of a base pair between Dz31-(G8A) and its substrate [b2a2-(C10U)] (Figure 1).

We calculated the kinetic parameters of the DNA enzymes by performing RNA-cleavage reactions under single- and multiple-turnover conditions. The cleavage products were analyzed by electrophoresis on a 20% polyacrylamide/7 M urea denaturing gel, as shown in Figure 4. The reactions with Dz31 and Dz31-(G8deaza) under single-turnover conditions were performed in 50 mM Tris–HCl (pH 8.0) plus 25 mM Mg^{2+} at 37°C. We used a lower pH, namely pH 6.0, for Dz31-(G8A) in order to slow down the rates of reactions so that we could make accurate measurements of kinetic parameters under single-turnover conditions in 50 mM Bis-Tris–HCl (pH 6.0). To obtain the kinetic parameters K_m and k_{cat} under single-turnover conditions, we used the equation $k_{obs} = k_{cleav} - (k_{obs} \times K_d)/[E]$ (Figure 5A–C) and the results are summarized in Table 1.

The mixtures for multiple-turnover reactions contained 0.5–10 μM DNA enzyme [Dz31 or Dz31-(G8deaza)] plus 1–50 μM b2a2 mRNA and 0.05–1 μM Dz31-(G8A) plus

Table 1. Kinetic parameters of cleavage of an RNA (17mer) substrate

Enzyme	Substrate	k_{cat} (min^{-1})	K_m (μM)
Dz31 (31mer)	b2a2 (17mer)	0.020 ± 0.003	1.89 ± 0.35
Dz31-(G8A) (31mer)[a]	b2a2-(C10U) (17mer)	0.050 ± 0.003	0.96 ± 0.12
Dz31-(G8deaza) (31mer)	b2a2 (17mer)	0.016 ± 0.001	0.11 ± 0.02

Determined in 50 mM of Tris–HCl (pH 8.0) and 25 mM of $MgCl_2$ under enzyme-saturating (single-turnover) conditions at 37°C.
[a]pH was 6.0.

Table 2. Kinetic parameters of cleavage of an RNA (17mer) substrate

Enzyme	Substrate	k_{cat} (min^{-1})	K_m (μM)
Dz31 (31mer)	b2a2 (17mer)	0.050 ± 0.013	8.20 ± 0.30
Dz31-(G8A) (31mer)	b2a2-(C10U) (17mer)	2.34 ± 0.02	2.93 ± 0.35
Dz31-(G8deaza) (31mer)	b2a2 (17mer)	0.10 ± 0.01	4.30 ± 0.51

Determined in 50 mM of Tris–HCl (pH 8.0) and 25 mM of $MgCl_2$ under multiple-turnover conditions at 37°C.

0.5–15 μM b2a2-(C10U) mRNA. All these reactions were performed in 50 mM Tris–HCl (pH 8.0) plus 25 mM Mg^{2+} ions at 37°C. Cleavage rates were obtained from the initial slopes of the curves of the time courses of reactions, and K_m and k_{cat} were calculated from Eadie–Hofstee plots (Figure 5D–F). The results are summarized in Table 2.

The K_m values of Dz31-(G8deaza) and Dz31-(G8A) were smaller than that of Dz31, as shown in Tables 1 and 2. Since Dz31-(G8deaza) and Dz31-(G8A) do not form quadruplexes, they can bind easily to their substrates. In contrast, Dz31 can form a quadruplex and, thus, the association of the DNA enzyme with its substrate is impaired. Since the preformed G-quadruplex seemed to be extremely stable (inert), it is difficult to unfold Dz31-quadruplex to accommodate its substrate RNA (33). As a result, the observed K_m of Dz31 was larger than those of Dz31-(G8deaza) and Dz31-(G8A). The k_{cat} value of Dz31-(G8deaza) was similar to that of Dz31, as shown in Tables 1 and 2. This result is reasonable since k_{cat} reflects the cleavage rate under saturating conditions, implying that the formation of a G-quadruplex does not affect the chemical step during cleavage.

The k_{cat} value of Dz31-(G8A) was much higher than that of Dz31 and Dz31-(G8deaza), as shown in Figure 4 and summarized in Tables 1 and 2. The cleavage reaction catalyzed by Dz31-(G8A) was too fast for measurements of kinetic parameters at pH 7 and 8, and the reaction seemed to be pH dependent, as is the case for reactions catalyzed by hammerhead ribozymes (3,34). The difference between the reactions catalyzed by Dz31-(G8deaza) and Dz31-(G8A) involves the difference in sequence at position 8 in the DNA enzyme and the complementary sequence in the substrate. In the former case, there is an N^7-deazaG–C base pair and in the latter case there is an A–U base pair. In neither case does a quadruplex form. The different base pairs produce extremely different k_{cat} values that reflect the chemical step during cleavage. It is possible that the combination of the A–U base pair moves the conformation in the vicinity of the catalytic site closer to the transition state with lower energy and, thus, the A–U base pair is more effective than the G–C base pair at this position (35).

It seems probable that the difference in kinetic parameters between Dz31 and Dz31-(G8A), as shown in Tables 1 and 2, was due to at least two factors: (i) the formation of a G-quadruplex, which affects K_m and (ii) the conformation in the transition state, which affects k_{cat}.

CONCLUSION

We have analyzed in detail the formation of quadruplexes by DNA oligomers. Adjacent G residues, even if they are within the catalytic site of the DNA enzyme, form a G-quadruplex, as indicated by gel mobility, CD measurements and kinetic parameters. Addition of negative charges (phosphorylation) to the ends of G-quadruplex-forming oligomers inhibited dimerization of G-quadruplexes. To our knowledge, this is the first example of inhibition of the dimerization of G-quadruplexes by direct phosphorylation of a continuous terminal stretch of G residues. Furthermore, we compared the catalytic activities of Dz31 and its mutant derivatives, such as Dz31-(G8A) and Dz31-(G8deaza), in which hydrogen bonding within the stretch of G residues was disrupted. The values of k_{cat} for Dz31 and Dz31-(G8deaza) were almost the same under single-turnover conditions, but Dz31-(G8deaza) was a slightly more efficient catalyst under multiple-turnover conditions, reflecting the presence of a higher concentration of a more reactive species in the latter case. Dz31-(G8A), which did not form a G-quadruplex and possessed the favorable A–U base pair, was 50 times more reactive than Dz31 and Dz31-(G8deaza). Reflecting the formation of a G-quadruplex, Dz31 had a significantly higher K_m than Dz31-(G8A) and Dz31-(G8deaza). As expected, G-quadruplexes within DNA enzymes inhibited catalysis and, thus, selection of corresponding target sequences should be avoided in an effort to maintain high rates of cleavage by DNA enzymes.

ACKNOWLEDGEMENTS

The authors thank Ms Clair Price for critical reading of the manuscript. M.K.U. was supported by the Japan Society for the Promotion of Science (JSPS).

REFERENCES

1. Bock,L.C., Griffin,L.C., Latham,J.A., Vermaas,E.H. and Toole,J.J. (1992) Selection of single-stranded DNA molecules that bind and inhibit human thrombin. *Nature*, 355, 564–566.
2. Ellington,A.D. and Szostak,J.W. (1992) Selection *in vitro* of single-stranded DNA molecules that fold into specific ligand-binding structures. *Nature*, 355, 850–852.
3. He,Q.-C., Zhou,J.-M., Zhou,D.-M., Nakamatsu,Y., Baba,T. and Taira,K. (2002) Comparison of metal-ion-dependent cleavages of RNA by a DNA enzyme and a hammerhead ribozyme. *Biomacromolecules*, 3, 69–83.
4. Cuenoud,B. and Szostak,J.W. (1995) A DNA metalloenzyme with DNA ligase activity. *Nature*, 375, 611–614.
5. Carmi,N., Shultz,L.A. and Breaker,R.R. (1996) *In vitro* selection of self-cleaving DNAs. *Chem. Biol.*, 3, 1039–1046.

6. Li,Y. and Sen,D. (1997) Toward an efficient DNA enzyme. *Biochemistry*, **36**, 5589–5599.
7. Li,Y. and Breaker,R.R. (1999) Deoxyribozymes: new players in the ancient game of biocatalysis. *Curr. Opin. Struct. Biol.*, **9**, 315–323.
8. Li,Y., Liu,Y. and Breaker,R.R. (2000) Capping DNA with DNA. *Biochemistry*, **39**, 3106–3114.
9. Feldman,A.R. and Sen,D. (2001) A new and efficient DNA enzyme for the sequence-specific cleavage of RNA. *J. Mol. Biol.*, **313**, 283–294.
10. Wang,D.Y., Lai,B.H.Y., Feldman,A.R. and Sen,D. (2002) A general approach for the use of oligonucleotide effectors to regulate the catalysis of RNA-cleaving ribozymes and DNA enzymes. *Nucleic Acids Res.*, **30**, 1735–1742.
11. Breaker,R.R. and Joyce,G.F. (1994) A DNA enzyme that cleaves RNA. *Chem. Biol.*, **1**, 223–229.
12. Santoro,S.W. and Joyce,G.F. (1997) A general purpose RNA-cleaving DNA enzyme. *Proc. Natl Acad. Sci. USA*, **94**, 4262–4266.
13. Cox,J.C., Cohen,D.S. and Ellington,A.D. (1999) The complexities of DNA computation. *Trends Biotechnol.*, **17**, 151–154.
14. Kuwabara,T., Warashina,M., Tanabe,T., Tani,K., Asano,S. and Taira,K. (1997) Comparison of the specificities and catalytic activities of hammerhead ribozymes and DNA enzymes with respect to the cleavage of *BCR-ABL* chimeric L6 (b2a2) mRNA. *Nucleic Acids Res.*, **25**, 3074–3081.
15. Warashina,M., Kuwabara,T., Nakamatsu,Y. and Taira,K. (1999) Extremely high and specific activity of DNA enzymes in cells with Philadelphia chromosome. *Chem. Biol.*, **6**, 237–250.
16. Santoro,S.W. and Joyce,G.F. (1998) Mechanism and utility of an RNA-cleaving DNA enzyme. *Biochemistry*, **37**, 13330–13342.
17. Nowell,P.C. and Hungerford,D.A. (1960) A minute chromosome in human chronic granulocytic leukemia. *Science*, **132**, 1497–1499.
18. Blackburn,E.H. (1994) Telomeres: no end in sight. *Cell*, **77**, 621–623.
19. Sen,D. and Gilbert,W. (1988) Formation of parallel four-stranded complexes by guanine-rich motifs in DNA and its implications for meiosis. *Nature*, **334**, 364–366.
20. Evans,T., Schon,E., Gora-Maslak,G., Patterson,J. and Efstratiadis,A. (1984) S1-hypersensitive sites in eukaryotic promoter regions. *Nucleic Acids Res.*, **12**, 8043–8058.
21. Kilpatrick,M.W., Torri,A., Kang,D.S., Engler,J.A. and Wells,R.D. (1986) Unusual DNA structures in the adenovirus genome. *J. Biol. Chem.*, **261**, 11350–11354.
22. Fry,M. and Loeb,L.A. (1994) The fragile X syndrome d(CGG)$_n$ nucleotide repeats form a stable tetrahelical structure. *Proc. Natl Acad. Sci. USA*, **91**, 4950–4954.
23. Williamson,J.R. (1993) Guanine quartets. *Curr. Opin. Struct. Biol.*, **3**, 357–362.
24. Williamson,J.R. (1994) G-quartet structures in telomeric DNA. *Annu. Rev. Biophys. Biomol. Struct.*, **23**, 703–730.
25. Keniry,M.A. (2001) Quadruplex structures in nucleic acids. *Biopolymers*, **56**, 123–146.
26. Henderson,E., Hardin,C.C., Walk,S.K., Tinoco,J.I. and Blackburn,E.H. (1987) Telomeric DNA oligonucleotides form novel intramolecular structures containing guanine–guanine base pairs. *Cell*, **51**, 899–908.
27. Gueschlbauer,W., Chantot,J.-F. and Thiele,D. (1990) Four-stranded nucleic acid structures 25 years later: from guanosine gels to telomer DNA. *J. Biomol. Struct. Dyn.*, **8**, 491–511.
28. Balagurumoorthy,P. and Brahmachari,S.K. (1994) Structure and stability of human telomeric sequence. *J. Biol. Chem.*, **269**, 21858–21869.
29. Penazova,H. and Vorlickova,M. (1997) Guanine tetraplex formation by short DNA fragments containing runs of guanine and cytosine. *Biophys. J.*, **73**, 2054–2063.
30. Protozanova,E. and Macgregor,R.,Jr (1996) Frayed wires: a thermally stable form of DNA with two distinct structural domains. *Biochemistry*, **35**, 16638–16645.
31. Sen,D. and Gilbert,W. (1992) Novel DNA superstructures formed by telomere-like oligomers. *Biochemistry*, **31**, 65–70.
32. Wang,Y. and Patel,D.J. (1992) Guanine residues in d(T_2AG_3) and d(T_2G_4) form parallel-stranded potassium cation stabilized G-quadruplexes with anti glycosidic torsion angles in solution. *Biochemistry*, **31**, 8112–8119.
33. Li,W., Miyoshi,D., Nakano,S. and Sugimoto,N. (2003) Structural competition involving G-quadruplex DNA and its complement. *Biochemistry*, **42**, 11736–11744.
34. Takagi,Y., Warashina,M., Stec,W.J., Yoshinari,K. and Taira,K. (2001) Recent advances in the elucidation of the mechanisms of action of ribozymes. *Nucleic Acids Res.*, **29**, 1815–1834.
35. Cairns,M.J., King,A. and Sun,L.-Q. (2003) Optimization of the 10–23 DNAzyme-substrate pairing interactions enhanced RNA cleavage activity at purine–cytosine target sites. *Nucleic Acids Res.*, **31**, 2883–2889.

The EMBO Journal (2004) 23, 959–968 | © 2004 European Molecular Biology Organization | All Rights Reserved 0261-4189/04
www.embojournal.org

THE EMBO JOURNAL

An RNA-dependent protein kinase is involved in tunicamycin-induced apoptosis and Alzheimer's disease

Reiko Onuki[1,2,3,10], Yoshio Bando[4,5,6,10], Eigo Suyama[1,7,8], Taiichi Katayama[5,6,9], Hiroaki Kawasaki[1,7], Tadashi Baba[3], Masaya Tohyama[5,6] and Kazunari Taira[1,7,*]

[1]Gene Function Research Center, National Institute of Advanced Industrial Science and Technology, Higashi, Tsukuba Science City, Japan, [2]Department of Molecular Pharmacokinetics, Graduate School of Pharmaceutical Sciences, The University of Tokyo, Tokyo, Japan, [3]Graduate School of Life and Environmental Sciences, University of Tsukuba, Tennoudai, Tsukuba Science City, Japan, [4]Department of Anatomy I, Asahikawa Medical College, Midorigaoka-higashi, Asahikawa, Hokkaido, Japan, [5]Department of Anatomy and Neuroscience, Graduate School of Medicine, Osaka University, Yamada-oka, Suita, Osaka, Japan, [6]Core Research for Evolutional Science and Technology, Japan Science and Technology, Saitama, Japan, [7]Department of Chemistry and Biotechnology, School of Engineering, The University of Tokyo, Hongo, Tokyo, Japan, [8]Genomics Institute of the NovarTis Reserch Foundation, San Diego, CA, USA, and [9]Center for Research in Neurodigenerative Diseases, Toronto, Ontario, Canada

Various types of stress, such as disruption of calcium homeostasis, inhibition of protein glycosylation and reduction of disulfide bonds, result in accumulation of misfolded proteins in the endoplasmic reticulum (ER). The initial cellular response involves removal of such proteins by the ER, but excessive and/or long-term stress results in apoptosis. In this study, we used a randomized ribozyme library and ER stress-mediated apoptosis (tunicamycin-induced apoptosis) in SK-N-SH human neuroblastoma cells as a selective phenotype to identify factors involved in this process. We identified a double-stranded RNA-dependent protein kinase (PKR) as one of the participants in this process. The level of nuclear PKR was elevated, but the level of cytoplasmic PKR barely changed in tunicamycin-treated SK-N-SH cells. Furthermore, tunicamycin also raised levels of phosphorylated PKR in the nucleus. We also detected the accumulation of phosphorylated PKR in the nuclei of autopsied brain tissues in Alzheimer's disease. Thus, PKR might play a role in ER stress-induced apoptosis and in Alzheimer's disease.

The EMBO Journal (2004) **23**, 959–968. doi:10.1038/sj.emboj.7600049; Published online 5 February 2004
Subject Categories: molecular biology of disease; neuroscience
Keywords: Alzheimer's disease; ER stress; neuronal degenerative diseases; PKR; ribozyme

*Corresponding author. Department of Chemistry and Biotechnology, School of Engineering, The University of Tokyo, 7-3-1 Hongo, Bunkyo-ku, Tokyo 113-8656, Japan. Tel.: +81 3 5841 8828 or +81 29 861 3015; Fax: +81 3 5841 8828 or +81 29 861 3019;
E-mail: taira@chembio.t.u-tokyo.ac.jp
[10]These authors contributed equally to this work

Received: 1 October 2002; accepted: 18 November 2003; Published online: 5 February 2004

Abbreviations: ER, endoplasmic reticulum; AD, Alzheimer's disease; Rz, hammerhead ribozyme; Tm, tunicamycin; GRP, glucose-regulated protein; PKR, double-stranded RNA-dependent protein kinase; PACT, PKR-activating protein; eIF2α, eucaryotic translation initiation factor subunit 2α; EBV, Epstein–Barr virus; GAPDH, glyceraldehyde-3-phosphate dehydrogenase; TUNEL, TdT-mediated dUTP nick end-labeling; Aβ, amyloid β peptide; PBS, phosphate-buffered saline; WT, wild type; DN, dominant negative

Introduction

Approximately one-third of newly synthesized proteins, in particular, transmembrane and secretory proteins, are transported to the lumen of the endoplasmic reticulum (ER). Many post-translational modifications, including folding and oligomerization of such proteins, which are destined for distal compartments in the secretory pathway, occur in the ER. The ER also functions as an efficient quality-control system, and one of its roles is to prevent incompletely folded molecules from moving along secretory pathways. However, some forms of cellular stress (known collectively as ER stress), such as depletion of calcium ions from the ER lumen, inhibition of protein glycosylation, reduction of disulfide bonds, expression of mutant proteins and ischemic insults, lead to the accumulation of unfolded proteins in the ER (Kozutsumi *et al*, 1988; Kaufman, 1999).

Misfolding of proteins triggers three compensatory responses: the unfolded protein response, which is mediated by increased expression of molecular chaperones, such as GRP94 (GRP: glucose-regulated protein) and GRP78/Bip, which promote the proper folding of proteins (Mori, 2000; Urano *et al*, 2000); the generalized suppression of translation (Harding *et al*, 1999); and ER-associated degradation (Ng *et al*, 2000). These three protective responses act transiently to control the accumulation of misfolded proteins within the ER, but sustained ER stress leads to apoptosis, with the characteristic fragmentation of nuclei, condensation of chromatin and shrinkage of cell bodies (Imaizumi *et al*, 2001).

It appears that ER stress is associated with certain genetic and/or neuronal degenerative diseases, such as Alzheimer's disease (AD). Several possible pathogenic mechanisms have been proposed for AD, including mutations in or expression of alternatively spliced variants of presenilin, impairment of the signaling of ER stress and increased sensitivity to stress-induced apoptosis (Katayama *et al*, 1999, 2001; Sato *et al*, 1999, 2001).

Hammerhead ribozymes (Rzs) are catalytic RNA molecules that bind to and cleave defined complementary target RNAs (Uhlenbeck, 1987; Haseloff and Gerlach, 1988; Symons, 1992; Zhou and Taira, 1998). Rz-mediated cleavage requires a NUX triplet in the target RNA (where N can be any

ribonucleotide and X can be A, U or C; Zhou and Taira, 1998). This strict specificity allows the use of Rzs for suppression of the expression of specific genes, and a reverse functional genomic approach to gene discovery has been established that exploits randomized Rz libraries (Kruger *et al*, 2000; Welch *et al*, 2000; Kawasaki *et al*, 2002; Kawasaki and Taira, 2002; Chatterton *et al*, 2004; Nelson *et al*, 2003).

An Rz-mediated change in the phenotype of cells allows rapid identification of genes responsible for that particular phenotype. Using this technology, we have identified genes that are related to specific diseases (Kawasaki *et al*, 2004; Kawasaki and Taira, 2002; Onuki *et al*, 2002; Suyama *et al*, 2003a, b) and some functional microRNAs (Kuwabara *et al*, unpublished data; Kawasaki *et al*, 2004). However, the isolation of active Rzs requires the design of a suitable selection system in each case.

To identify genes involved in AD, we focused on genes that facilitate tunicamycin-induced (Tm-induced) ER stress-mediated apoptosis. We constructed an Rz-screening system for the isolation of genes that function in Tm-mediated apoptosis and identified the gene for a double-stranded RNA (dsRNA)-dependent protein kinase (PKR). We found that Tm-mediated ER stress promoted the activation of PKR in the human neuroblastoma cell line SK-N-SH. PKR, an interferon-induced protein kinase, was identified initially in a study of responses to viral infection. It is activated by the extensive secondary structure of the viral RNA (Gale and Katze, 1998). Upon binding to dsRNA, PKR is autophosphorylated and increases cellular sensitivity to apoptotic and/or proinflammatory stimuli through a number of putative pathways, which include the phosphorylation of eucaryotic translation initiation factor subunit 2α (eIF2α) which, in turn, blocks protein synthesis (Wu and Kaufman, 1997; Srivastava *et al*, 1998). PKR is involved in apoptosis that is induced not only by viral infection but also by, for example, the addition or removal of specific growth factors, lipopolysaccharide or Ca^{2+} ions (Prostko *et al*, 1995; Srivastava *et al*, 1995, 1998).

We examined the localization of PKR in Tm-treated SK-N-SH cells and found that levels of PKR were significantly elevated in the nuclei, where PKR formed aggregates. Furthermore, the level of phosphorylated PKR, an activated form, was also elevated in a nuclear fraction. We found PKR in the cell nuclei of autopsied brain tissue from AD patients, and the level of phosphorylated PKR was significantly higher than in the nuclear fractions from disease-free controls. Our results suggest a relationship between the activation of PKR and neuronal cell death in AD.

Results

Identification of genes involved in Tm-induced apoptosis using a randomized ribozyme library

To identify genes involved in ER stress, we used a simple apoptotic phenotype-based selection system, designed to select Rzs that suppress the expression of proapoptotic genes (Kawasaki *et al*, 2002; Kawasaki and Taira, 2002). As shown schematically in Figure 1A, human neuroblastoma SK-N-SH cells were transiently transfected with a randomized Rz library. After 24 h, cells were treated with Tm (2 μg/ml) for another 24 h as the first round of selection. This treatment caused apoptosis in most of the empty vector-transfected cells, and we isolated Rz-expressing plasmids from cells that survived the first round of transfection with the randomized ribozyme library. We amplified the isolated plasmids in bacteria and sequenced them. In the second round, cells were transfected with the recovered Rzs and exposed to Tm for a longer period (48 h) to eliminate 'weak positives'. The Rzs isolated after the second round of exposure to Tm were also amplified in bacteria. *Escherichia coli* transformants that contained the individual Rz expression plasmids appeared about five times more frequently than empty vector-transfected 'mock' cells after the first round (Figure 1B). Furthermore, the ratio of surviving Rz-containing cells and empty vector-transfected cells was about seven to one after the second round (Figure 1B). These results suggested that the frequency of false positives was reduced after the second round.

As we selected cells that transiently expressed Rzs, we could not exclude the possibility that these cells might contain multiple Rzs. Multiple ribozymes might inhibit cell death cooperatively or only one might suppress cell death. To examine the individual effects of each selected Rz, we tried to construct Epstein–Barr virus-based (EBV-based) expression vectors to generate semistable cell lines. EBV-based vectors can replicate autonomously in mammalian cells and we established 15 semistable lines of cells (Figure 1C; lines EB1-45, EB1-47, EB1-49, EB1-84 and EB1-130 were obtained after the first round of screening; lines EB2-16, EB2-23, EB2-30, EB2-31, EB2-53, EB2-68, EB2-76, EB2-117, EB2-131 and EB2-156 were obtained after the second round of screening). To confirm the effects of each Rz, we treated each cell line with Tm for 24 h and then examined apoptosis by TdT-mediated dUTP nick end-labeling (TUNEL) staining. In addition, we used mock-transfected cells as a control. We counted positive cells after TUNEL staining and calculated the proportion of apoptotic cells (Figure 1C). The EB1-84, EB2-16 EB2-30, EB2-31, EB2-76 and EB2-131 clones were slightly resistant to Tm-induced apoptosis. Moreover, the Rzs expressed by clones EB1-45, EB1-47, EB1-49, EB1-130, EB2-23, EB2-53, EB2-68, EB2-117 and EB2-156 effectively suppressed Tm-induced cell death, as compared to cell death in Tm-treated control cells. These results indicated that our screening system had allowed efficient and easy selection of Rzs that suppressed the activities of proapoptotic mRNAs in Tm-induced apoptosis.

As caspase-3 is activated in Tm-treated apoptotic cells, we also confirmed the viability of EB1-47 and EB2-68 by measuring the activity of caspase-3 (Siman *et al*, 2001). In both EB1-47 and EB2-68 cells, caspase-3 activity was significantly lower than that in mock-transfected cells and it was similar to that in z-VAD-fmk-treated cells (Figure 1D). It appeared that expression of each Rz completely inhibited activation of caspase-3. These two clones were selected for further analysis.

Tm-mediated ER stress promotes the expression of PKR in SK-N-SH cells

We determined the sequences of the selected Rzs and identified their target genes using the BLAST search program. We focused on Rz 47 and Rz 68 from clones EB1-47 and EB2-68, and the sequences of the binding arms of these Rzs are shown in Figure 2A. The BLAST search suggested that these Rzs might be able to cleave PKR mRNA, with Rz 47 cleaving the first intron of the PKR transcript and Rz 68 cleaving PKR mRNA between nucleotides 700 and 714 (Figure 2A, arrows).

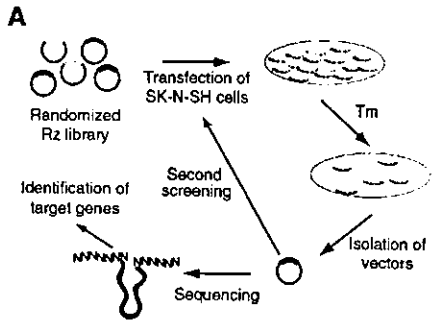

B

	Number of transformants		Ratio (Rz/mock)
	Mock	Rz library	
First	225	1191	5.3
Second	25	179	7.2

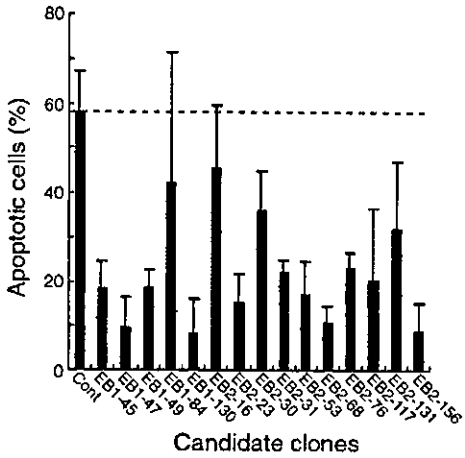

D

	Caspase 3-like activity (relative)	
	Control	Tm/24 h
Mock	1–0.1	6.5–0.25
EB1-47	1–0.1	2.8–0.67*
EB2-68	1–0.1	3.0–0.35**
z-VAD-fmk	1–0.1	3.8–1.12***

Means–s.d are shown (n=5)
* P>0.005; ** P>0.01; *** P>0.1

Figure 1 Selection of Rzs that suppress Tm-induced cell death from a randomized library. (**A**) Schematic representation of the selection system. (**B**) Number of transformants after each round of selection. Vectors isolated from surviving cells were introduced into DH5α. (**C**) Individual Rzs, selected from the randomized library, were examined for their ability to protect cells against Tm-mediated apoptosis. SK-N-SH cells that expressed selected Rzs were exposed to 2 μg/ml Tm for 24 h. Apoptosis was assessed by TUNEL staining. (**D**) The activation of caspase-3 depended on the activation of PKR. Cells were treated with Tm for 24 h or untreated (control), and then caspase-3 activity was measured. Cells treated with z-VAD-fmk were examined as controls.

We examined levels of Rz 47 and 68 in EB1-47 and EB2-68 cells and performed an analysis by RT–PCR with Rz-specific primers. Figure 2B shows that expression of each Rz was detectable in Rz-transfected cells but not in mock-transfected cells. To confirm the activities of Rz 47 and Rz 68 against the PKR transcript, we also performed analysis by RT–PCR using primers specific for genes for PKR and glyceraldehyde-3-phosphate dehydrogenase (GAPDH). The level of PKR rises and PKR is activated by dsRNA of more than 30 bp and these phenomena hindered the initial application of RNAi technology to mammalian cells (Elbashir *et al*, 2001; Miyagishi and Taira, 2002). As PKR might have been activated by expression of a ribozyme itself, we used Rz 49, which does not recognize PKR mRNA, as a control. After electrophoresis, we quantified levels of PKR mRNA and normalized them by reference to levels of GAPDH mRNA. As shown in Figure 2B, the expression of Rz 49 did not change the level of PKR mRNA from that in mock-transfected cells. However, the level of PKR mRNA in EB1-47 cells was 53% lower than that in empty vector-transfected cells (Figures 2B and C). Similar results were obtained in the case of Rz 68 (37% decrease).

We performed Western blotting analysis with anti-PKR or anti-Bax antibodies to determine levels of PKR in these cells (Figure 2D). We normalized levels of PKR by reference to levels of Bax. In Rz 47-expressing cells, 58% less PKR was expressed than in mock-transfected cells. Similar results were observed in Rz 68-expressing cells (Figure 2D). Thus, Rz 47 and Rz 68 specifically suppressed the expression of PKR at the post-transcriptional level.

Role of PKR in ER stress-induced apoptosis

Srivastava *et al* (1995) provided evidence that depletion of Ca^{2+} ions in the ER triggers stress signaling that might activate eIF2α kinase, a downstream effector of PKR. Thus, elucidation of the relationship between PKR and Tm-induced ER stress in SK-N-SH cells is clearly important. PKR is localized in both the cytoplasm and the nucleus (Jeffrey *et al*, 1995; Besse *et al*, 1998). To identify the role of PKR in vulnerability to ER stress, we prepared cytoplasmic and nuclear fractions from Tm-treated and nontreated cells and subjected them to Western blotting with anti-actin and anti-KDEL antibodies. In this experiment, we employed the level of actin (rather than the level of histone) as a loading control, because it was reported that degradation of histone was caused by apoptosis (Zhang *et al*, 2001). Anti-KDEL antibody interacts with molecular chaperones GRP94 and GRP78/Bip in the ER. Normal cells respond to ER stress by increasing the transcription of genes for chaperones, such as GRP94 and GRP78/Bip, in the ER. At first, we performed Western blotting using anti-histone or anti-actin antibodies to check whether the fractionation had worked well. The expression of histone was observed only in the nuclear fraction using wild type

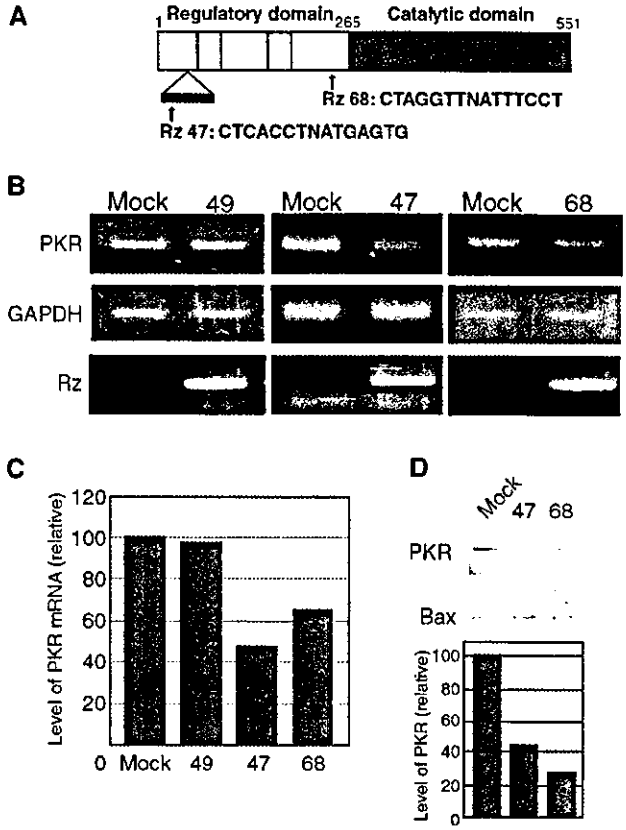

Figure 2 Rz 47 and Rz 68 suppress the expression of PKR. (**A**) Schematic illustration of candidate Rzs (Rz 47 and Rz 68) with binding sites and cleavage sites in the mRNA for PKR. Two gray boxes indicate dsRNA-binding motifs; white and black boxes indicate regulatory and catalytic domains, respectively. (**B**) Expression of PKR mRNA in cells transfected with the empty vector (mock) or the Rz 49, Rz 47 or Rz 68 expression vector. PKR mRNA was detected by RT-PCR with primers specific for PKR (upper). GAPDH mRNA served as an internal control (middle). Expression of Rzs was confirmed by RT-PCR with specific primers (lower). (**C**) Quantitative analysis of PKR mRNA. Levels of PKR mRNA were quantified and normalized by reference to levels of GAPDH mRNA. (**D**) Levels of PKR in three lines of cells as indicated. Extracts were subjected to Western blotting with anti-PKR (PKR) and anti-Bax antibodies (Bax). Results of quantitative analysis are also shown.

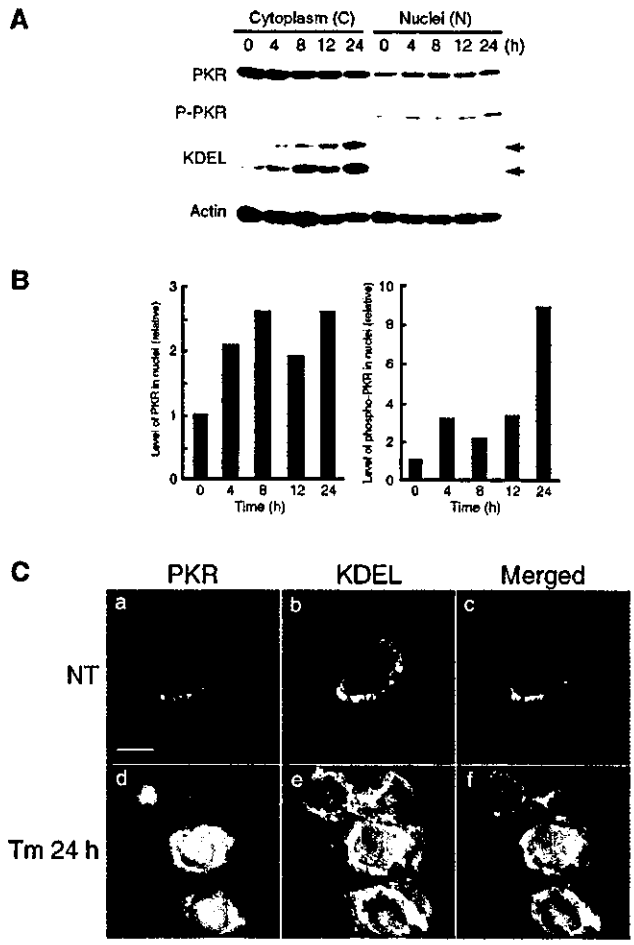

Figure 3 Subcellular localization of PKR and phosphorylated PKR in Tm-treated SK-N-SH cells. (**A**) Levels of nuclear PKR and phosphorylated PKR were elevated in SK-N-SH cells after exposure to ER stress (Tm: 2 μg/ml) for the indicated times. Cytoplasmic and nuclear fractions were subjected to Western blotting with anti-PKR, anti-phospho-PKR, anti-KDEL (upper arrow, GRP94; lower arrow, GRP78) and anti-actin antibodies as described in the text. (**B**) Relative intensities of bands (PKR and phosphorylated PKR) were normalized by reference to bands of β-actin. (**C**) Translocation of PKR to the nuclei in Tm-treated cells. Untreated (NT) and Tm-treated (2 μg/ml) cells were stained with anti-PKR and anti-KDEL antibodies (panels a and d, PKR, red; panels b and e, KDEL, green; panels c and f, overlapping images, yellow). Scale bar, 10 μm.

(WT) of cells; therefore, we used this method for further analysis (Supplementary Material 1).

Levels of actin remained unchanged but levels of GRP94 and GRP78/Bip in the cytoplasmic fraction increased after an 8-h incubation with Tm (Figure 3A), as described previously (Kozutsumi *et al*, 1988; Kaufman, 1999). Neither of these chaperones was detected in the nuclear fraction, suggesting that the nuclear fraction was not contaminated by cytoplasmic material, in agreement with the results shown in Supplementary Material 1. Western blotting analysis with anti-PKR and anti-phospho-PKR antibodies revealed that, when cells were stimulated with Tm for 8 h, the level of PKR rose in the nuclei (Figure 3A and left histogram in Figure 3B) while the level of cytoplasmic PKR barely changed.

Phosphorylation or cleavage of PKR is required for kinase activity. Using an anti-phospho-PKR antibody (which recognizes phosphorylation of Thr446), we detected phosphorylated PKR in the nuclear fraction, and the level of this form of PKR depended on the incubation time. The maximum level of phosphorylated PKR was detected 24 h after the start of treatment (Figure 3A and right histogram in Figure 3B).

When we examined the subcellular localization of PKR by immunofluorescence microscopy after SK-N-SH cells had been treated with Tm, we found most PKR (red) in untreated control in the cytoplasm (Figure 3C, upper left). After cells had been treated with Tm, levels of nuclear PKR increased and PKR was clearly localized in the nuclei (Figure 3C, lower left), while levels of GRP94 and GRP78/Bip (green) increased in the ER of treated cells (Figure 3C, middle). These results suggested that Tm-mediated ER stress promoted the expression of PKR in SK-N-SH cells.

Alanine-mutated PKR confers resistance to Tm

We investigated whether phosphorylated PKR might affect Tm-induced cell death. We constructed mutated PKR in

which threonine at residues 446 and 451 was changed to alanine. This mutant lacks an important phosphorylation site and acts as a dominant-negative (DN) protein (Jagus *et al*, 1999). SK-N-SH cells were transfected with the expression vector for DN-PKR or the empty vector. We also tried to establish cells expressing the WT PKR; however, overexpression of WT PKR caused apoptosis as described previously (Srivastava *et al*, 1995). Therefore, we employed mock-treated cells as a control. Selection yielded clones with the empty vector and the vector that encoded DN-PKR, namely, AlaC1 and AlaC2. We confirmed the expression of DN-PKR using anti-GFP antibody, since GFP was fused to PKR as a tag (Figure 4A).

We incubated AlaC1, AlaC2 and the control cells with Tm for 30 h and examined levels of cleaved caspase-3 (activated caspase-3). As shown in Figure 4B, small amounts of cleaved caspase-3 were detected in AlaC1 and AlaC2 clones, but a large amount of cleaved caspase-3 was detected in the mock-transfected clone. Levels of actin were used as internal controls that remained unchanged. Next, we incubated AlaC1, AlaC2 and mock cells with Tm for 24 h, and then performed TUNEL staining. As shown in Figure 4C, about 75% of cells that expressed DN-PKR survived, while only 20% of mock-transfected cells survived (Figure 4C), suggesting that expression of DN-PKR inhibited apoptosis.

Next, we examined the localization of PKR in cells that expressed DN-PKR (Figure 4D). Control and DN-PKR-expressing cells were incubated with Tm. Before treatment, most PKR was localized in the cytoplasm in both cell lines. After incubation, PKR was localized in the nuclei, while DN-PKR remained in the cytoplasm, suggesting that expression of mutated PKR changed the localization of PKR and inhibited apoptosis.

Levels of nuclear PKR in AD brain tissue

Considerable evidence suggests that ER stress is closely related to genetic and/or neuronal degenerative diseases, such as AD (Katayama *et al*, 1999, 2001; Sato *et al*, 1999, 2001; Imaizumi *et al*, 2001). Therefore, we examined levels of PKR in the autopsied brains of sporadic AD patients. We prepared crude nuclear and cytoplasmic fractions (for seven disease-free controls and 17 patients with AD) for Western blotting with anti-phospho-PKR and anti-actin antibodies. Phosphorylated PKR was barely detectable in the cytoplasmic fractions from AD tissues and tissues from age-matched controls (data not shown). Levels of phosphorylated PKR were significantly higher in crude nuclear fractions of AD tissues than of controls (Figure 5A; actin was used as a loading control). Levels of phosphorylated PKR were quantified and normalized by reference to levels of actin (Figure 5B). In most AD samples, the level of phosphorylated PKR was significantly higher than in age-matched control samples.

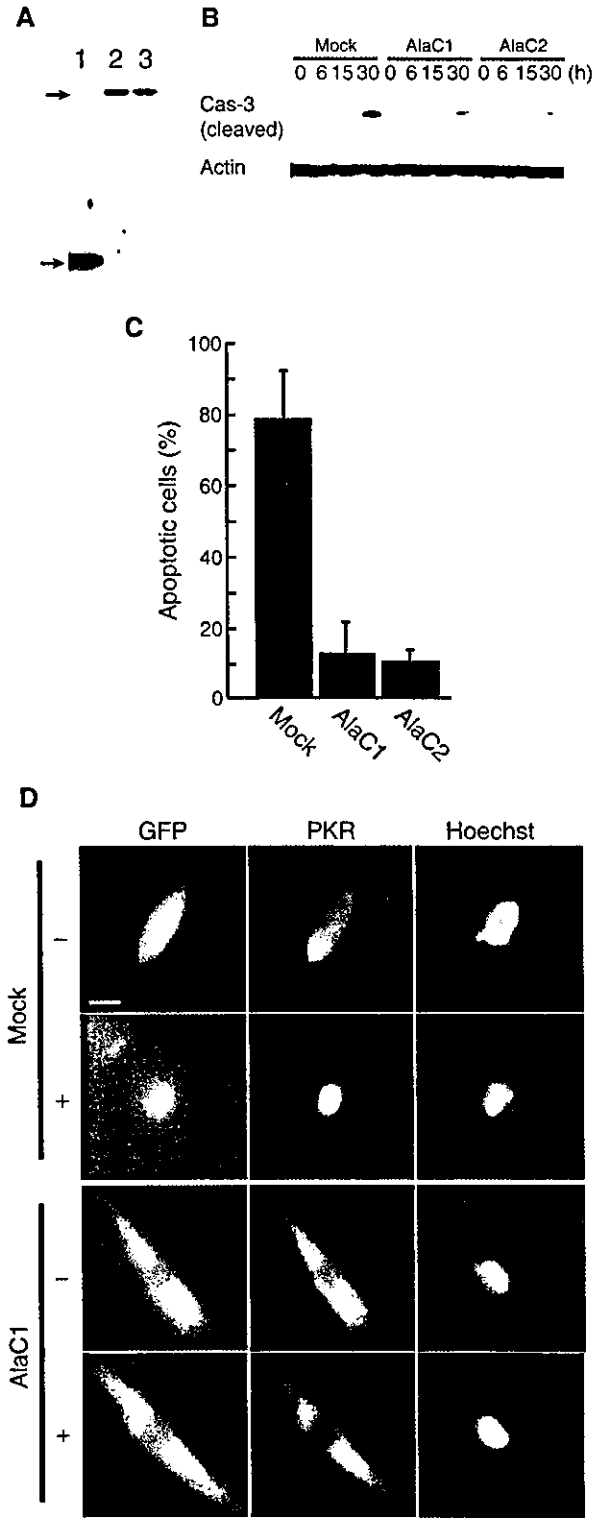

Figure 4 Expression of DN-PKR inhibits Tm-induced apoptosis. (**A**) Immunoblotting analysis of the expression of DN-PKR. Extracts of GFP-expressing cells (lane 1) and two independent clones (lanes 2 and 3) expressing DN-PKR fused to GFP were examined with anti-GFP antibody. The upper arrow indicates DN-PKR fused to GFP and the lower arrow indicates GFP. (**B**) Levels of activated caspase-3 in Tm-treated cells. Cells expressing GFP or GFP-DN-PKR were incubated with Tm (2 μg/ml), and activation of caspase-3 was examined by Western blotting with anti-cleaved caspase-3 antibody. Levels of β-actin were analyzed as an internal control. (**C**) Tm-mediated apoptosis is inhibited by expression of DN-PKR. Cells were treated with 2 μg/ml Tm for 24 h and apoptosis was assessed by TUNEL staining. (**D**) Localization of PKR and DN-PKR in Tm-treated cells. Untreated cells (−) and Tm-treated cells (+) were stained with anti-PKR antibody (PKR; red). Green fluorescence indicates DN-PKR; the nuclei were stained with Hoechst 33258 (blue). Scale bar, 10 μm.

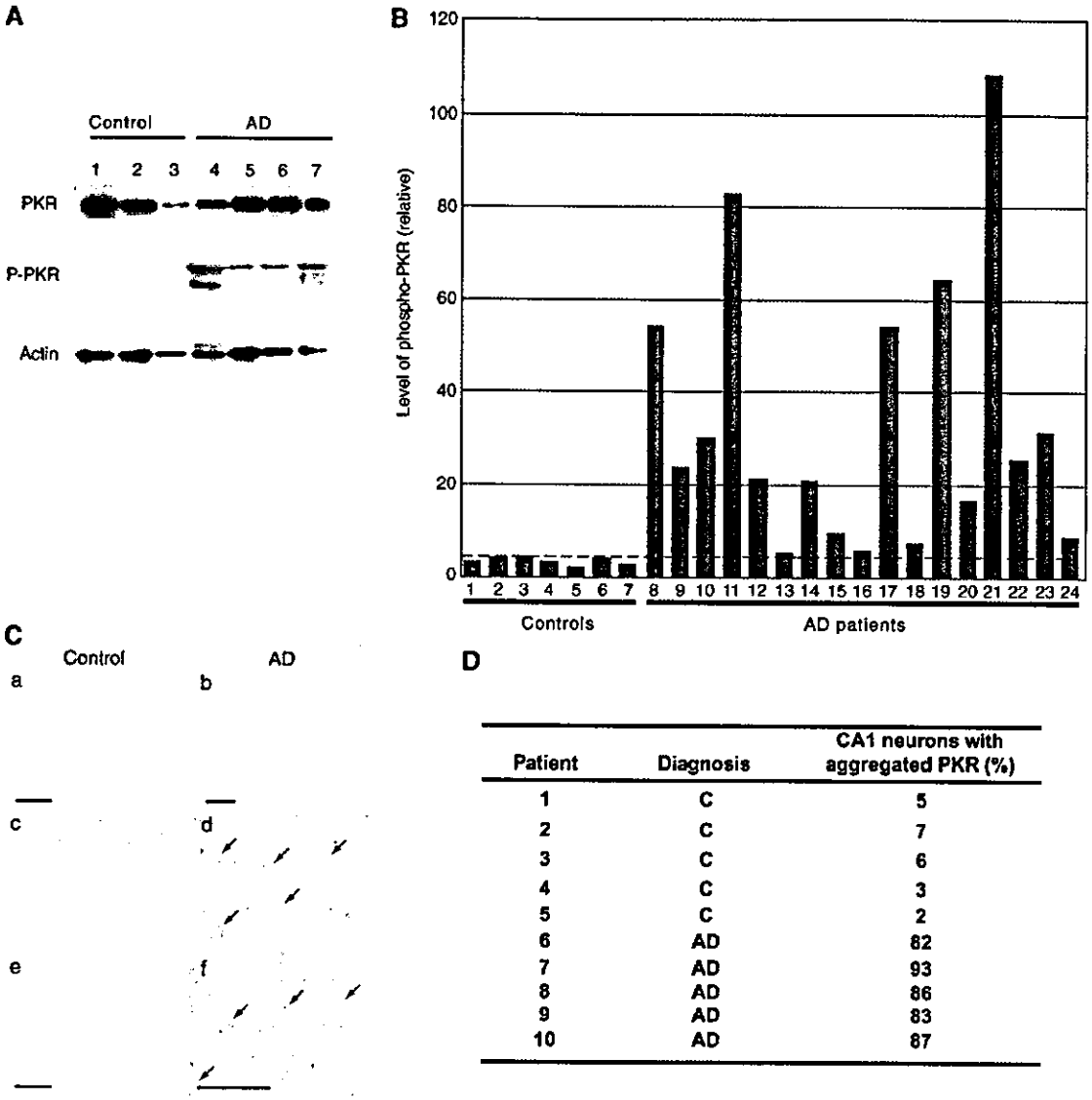

Patient	Diagnosis	CA1 neurons with aggregated PKR (%)
1	C	5
2	C	7
3	C	6
4	C	3
5	C	2
6	AD	82
7	AD	93
8	AD	86
9	AD	83
10	AD	87

Figure 5 PKR is concentrated in the nuclei and is phosphorylated in autopsied AD brains. (**A**) Levels of phosphorylated PKR in autopsied AD brains. Nuclear proteins in the extracts of temporal cortex from patients with AD (lanes 4–7) were subjected to Western blotting with anti-PKR (PKR), anti-phospho-PKR (P-PKR) and anti-actin (actin) antibodies. Controls were age-matched and are described in the text (lanes 1–3). (**B**) Quantitative analysis of levels of phosphorylated PKR, normalized by reference to levels of β-actin, in the temporal cortex. Numbers 1–7, disease-free controls; numbers 8–24, sporadic AD patients (AD). Numbers 1–3 correspond to lanes 1–3 and numbers 8–11 correspond to lanes 4–7 in (A). (**C**) Expression of PKR in AD autopsy tissue. Panels a, c and e show tissues from an age-matched control and panels b, d and f show tissues from an AD autopsy. Panels a and b, hippocampus; panels c and d, CA1 region; panels e and f, CA3 region. Arrows indicate nuclear aggregates of PKR. Scale bar: panels a and b, 100 μm; panels e and f, 10 μm. (**D**) Aggregated PKR in AD brains. Aggregated PKR was significantly more common in sporadic AD brains than in controls. AD, sporadic AD patient; C, age-matched control.

To study the localization of PKR, we examined the autopsied hippocampus of an AD patient. The hippocampus is affected early in the course of AD and has been studied extensively (Selkoe, 1994). Immunohistochemical analysis suggested that PKR immunoreactivity was slightly higher in the hippocampus of the AD patient than in the control (Figure 5C, panel a versus b). Under high magnification, PKR was observed specifically in the nuclei, in particular in the CA1 and CA3 regions (Figure 5C, panels d and f, arrows). Similar observations were made in all the three samples of AD tissue examined. In contrast, immunoreactive PKR in age-matched controls was detected only in the cytoplasm of cells (Figure 5C, panels c and e).

To determine the proportion of neurons with aggregated PKR in sporadic AD (five cases) and age-matched controls (non-neurological diseases; five cases), we performed an immunohistochemical analysis of sections of the hippocampal CA1 region in each case (Figure 5D). Aggregation of PKR was observed in all specimens from AD brains, and the proportion of positive neurons in AD brains was above 80%. In contrast, positive neurons accounted for only 2–7% of the total in age-matched controls. These results suggest that phosphorylation and aggregation of PKR in the nucleus of neurons might be associated with the pathology of AD.

Discussion

In this study, we developed a system for selection of Rzs that suppress the expression of proapoptotic genes that are involved in Tm-induced apoptosis (Figures 1A and B). To

confirm the activity of 10 selected Rzs, we performed TUNEL staining after treatment of Rz-expressing cells with Tm. As shown in Figure 1C, most of the selected Rzs conferred resistance against Tm-induced apoptosis. However, we could not eliminate contamination by false-positive clones after the second selection. This observation suggested that Tm failed to cause apoptosis uniformly and that a small fraction of cells was able to avoid apoptosis in the absence of active Rzs. Thus, to confirm the reproducibility of the effect of each selected Rz on Tm-induced apoptosis, we used EBV-based vectors to express each individual Rz for a third round of selection and further analysis.

EBV-based vectors are extrachromosomal vectors that replicate autonomously in mammalian cells, but not in rodent cells, and they are distributed to both daughter cells after cytokinesis (Tanaka *et al*, 1999). Such vectors are never inserted into the host genome and, thus, the level of Rz expression remains constant in each transfected cell and it is not necessary to select multiple clones for analysis of a specific Rz.

Using semistable EBV-transfected clones, we performed TUNEL staining as a third selection to eliminate weak positives (Figure 1C). Our established protocol allowed the efficient and easy selection of active Rzs from the randomized library, and the selected Rzs suppressed ER stress-mediated apoptosis. As each Rz binds to and cleaves a defined RNA that has a complementary target sequence, the sequences of the substrate-binding arms of the selected Rzs allowed us to identify ER stress-related genes using a computerized search program.

The results of the third selection and the assay of caspase-3 activity focused our attention on Rz 47 and Rz 68, which appeared to target PKR mRNA (Figures 1C and D). dsRNAs of more than 30 bp bind to and activate PKR. To examine whether expression of Rzs could, itself, activate PKR, we performed RT–PCR using Rz 49-expressing cells (Rz 49 does not recognize PKR mRNA). As shown in Figures 2B and C, levels of PKR mRNA were the same in mock-transfected cells and Rz 49-transfected cells. Thus, a nonspecific Rz did not activate PKR. Cells expressing Rz 47 and Rz 68 efficiently suppressed the expression of PKR mRNA, as indicated by RT–PCR (Figures 2B and C) and so we selected these two clones for further analysis.

We examined the role of PKR in Tm-mediated ER stress using WT SK-N-SH cells and their Rz-expressing derivatives. In general, PKR is expressed in an inactive state. However, when cells are subjected to certain stresses, two independent pathways activate PKR. One involves the autophosphorylation of PKR after the binding of dsRNA (Gale and Katze, 1998) or a dsRNA-independent activator, PKR-activating protein (PACT) (Prostko *et al*, 1995; Patel and Sen, 1998; Patel *et al*, 2000; Peters *et al*, 2001). The other involves caspase-catalyzed cleavage of PKR between its regulatory and kinase domains (Satoh *et al*, 1999; Saelens *et al*, 2001), without a requirement for phosphorylation.

As shown in Figure 3, we analyzed the relationship between activation of PKR and Tm-induced ER stress in WT SK-N-SH cells. When ER stress was induced by Tm, the level of PKR or of phosphorylated PKR increased in the nuclei (Figures 3A and B), but no caspase-dependent cleavage of PKR was detected (data not shown). We also examined levels of PACT, which remained unchanged during Tm-induced cell death (data not shown).

We examined whether phosphorylation of PKR is necessary for apoptosis. We constructed a DN form of PKR (DN-PKR) in which Thr446 and Thr451 were changed to alanine, since phosphorylation of these two residues is critical for activation of PKR (Jagus *et al*, 1999). Two independent clones expressing DN-PKR were resistant to Tm-induced cell death (Figures 4A–C). Therefore, activation of PKR seemed to depend on its phosphorylation, and only phosphorylated PKR acted as a proapoptotic factor in Tm-induced apoptosis. We did not, however, identify any specific activator that binds to PKR. We also established a cell line that overexpressed PKR fused to GFP as a tag. We monitored the localization of PKR during Tm-induced apoptosis in these cells, as shown in Figure 4D. We failed to establish cell lines that overexpressed intact PKR because overexpression of PKR leads to apoptosis, as described previously (Srivastava *et al*, 1998). As shown in 'Supplementary Material 2', we observed the localization of WT PKR fused with GFP transiently. In control cells (expressing GFP protein), fluorescence of GFP diffused both in the nucleus and the cytoplasm. WT PKR fused with GFP also localized in the nucleus and the cytoplasm; however, the nuclear PKR seemed to aggregate like those in Tm-induced WT cells (Figures 3C, panel d). Furthermore, this localization is clearly different from that of DN-PKR-expressing cells. These results suggest that GFP fusing does not inactivate PKR activity. In addition, transient expression of WT PKR fused with GFP also caused apoptosis (data not shown).

In a recent report, we suggested that a relationship might exist between stress, at the level of the ER, and neuronal cell death in AD (Katayama *et al*, 1999). It has been reported that caspase-12 is localized in the ER and is activated by ER stress. In addition, caspase-12-deficient cortical neurons are defective in apoptosis that is induced by amyloid-β peptide (Aβ; a major constituent of senile plaques). Therefore, caspase-12 appears to mediate an ER-specific pathway to apoptosis and might contribute to the neurotoxicity of Aβ (Nakagawa *et al*, 2000; Nakagawa and Yuan, 2000). Thus, the apoptotic cascade that originates in the ER might play a critical role in neuronal cell death. For this reason, we compared PKR in the brains of AD patients with that in age-matched disease-free controls. As shown in Figures 5A and B, levels of phosphorylated PKR were significantly elevated in the nuclear fractions of AD brains, as they are in the nuclear fractions of Tm-treated SK-N-SH cells. Furthermore, we found aggregated PKR in the nuclei of samples from AD brains (Figures 5C and D). Although many cells showed aggregations of PKR in their nuclei, these cells had not, apparently, undergone apoptosis, as judged histochemically. It is possible that the aggregation of PKR in the nuclei occurs at an early phase in the pathogenesis of AD. We also detected elevated levels of PKR in the brains of patients, at autopsy, who had died of Huntington's disease or Parkinson's disease (data not shown; manuscript in preparation). It is possible that PKR might be widely involved in neuronal degenerative diseases.

In summary, we have identified PKR as a proapoptotic protein in Tm-induced apoptosis. During apoptosis, phosphorylation of PKR was elevated and phosphorylated PKR was localized in the nuclei of SK-N-SH cells. In the nuclei in AD brains, similar results underscore the potential importance of phosphorylated PKR.

Our libraries of randomized Rz and/or genome-wide specific siRNAs (Miyagishi and Taira, 2003), some of them

targeting micro RNAs (Kawasaki *et al*, 2004) should serve as powerful tools for the development of gene-suppressing reagents of both therapeutic and general importance and for the rapid identification of genes whose functions are of specific interest.

Materials and methods

Chemicals and antibodies

Tm was obtained from Sigma (Missouri). Anti-PKR (sc-9479; Santa Cruz Biotech., California), anti-Bax (sc-493; Santa Cruz Biotech.), anti-phospho-PKR (07-148; Upstate Biotech., New York), anti-KDEL (SPA-827; Stressgen Biotech., California), anti-cleaved caspase-3 antibody (Cell Signaling Technology, Massachusetts) and anti-actin (Chemicon International, California) antibodies were purchased for this study. Anti-GFP antibody was kindly provided by Dr Nagasaki (AIST, Ibaraki, Japan).

Culture and transfection of cells

SK-N-SH cells were grown in MEM-α (Invitrogen, The Netherlands) supplemented with 10% fetal calf serum (Invitrogen). Cells were transiently, semistably or stably transfected with plasmids using Lipofectamine™ 2000 (Invitrogen) according to the manufacturer's protocol. After transfection, cells were selected with Geneticin® (Sigma).

The randomized Rz expression library and construction of Rz expression vectors

The randomized Rz expression library was prepared in the vector pUC-dt, as described previously (Suyama *et al*, 2003a). The pEB6-CAG vector (EBV-based vector) was kindly provided by Dr Miwa (Tsukuba University, Ibaraki, Japan; Tanaka *et al*, 1999). It was digested with *Eco*RI and *Bam*HI and self-ligated. The Rz expression cassette that included the promoter of a human gene for $tRNA^{val}$ was inserted at the *Afl*III site of pEB6-CAG to generate pEBRz. The 10 recovered plasmids were digested with *Eco*RI and *Kpn*I, and fragments were inserted at the *Eco*RI/*Kpn*I site of pEBRz to generate vectors for semistable expression.

Screening for active ribozymes

Lines of SK-N-SH cells that had been transiently transfected with the randomized Rz library were treated with Tm (2 μg/ml). For the first screening, transfected cells were exposed to Tm for 24 h. For the second screening, cells were transfected with candidate plasmids from the first screening and collected after incubation with Tm for 48 h. Expression vectors harboring Rzs were isolated from surviving cells and used to transform DH5α (TOYOBO, Tokyo, Japan).

Detection of cell death or apoptosis

Lines of SK-N-SH cells that had been semistably transfected with Rz expression vectors were treated with Tm (2 μg/ml) for 24 h. Apoptotic cells were stained by TUNEL or propidium iodide. For TUNEL staining, SK-N-SH cells were fixed in 4% formaldehyde for 25 min at 4°C and then permeabilized by treatment with 0.2% Triton X-100 in phosphate-buffered saline (PBS) for 5 min. After three washes with PBS, cells were subjected to TUNEL staining with the DeadEND™ Fluorometric TUNEL System (Promega, Wisconsin) according to the manufacturer's protocol. Cells were observed under a conventional fluorescence microscope (LSM-510; Carl Zeiss, Germany). To monitor chromatin condensation, we incubated cells with Hoechst 33258 for 10 min, and examined them under the fluorescence microscope.

Measurement of caspase-3-like activity

Caspase-3-like activity was measured spectrophotometrically as described previously (Tamatani *et al*, 2000). In brief, cells that had been exposed to 2 μg/ml Tm for 24 h were suspended in ice-cold ICE buffer (50 mM Tris-HCl, pH 7.4, 1% NP-40, 1 mM PMSF, 1 mM EDTA and 10 mM EGTA) with subsequent centrifugation. The concentration of protein in the resulting supernatant was measured. Then, an aliquot of the supernatant, containing 40 μg of protein, was incubated with 50 μM substrate for caspase-3 (Ac-DEVD-MCA; Peptide Institute, Osaka, Japan) for 30 min at 37°C. The enzymatic activity was monitored by measuring absorbance (excitation, 380 nm; emission, 460 nm) in a spectrophotometer (F-3000; Hitachi, Tokyo, Japan). For experiments with an inhibitor of caspase-3, we used 1 μM z-VAD-fmk (Peptide Institute, Osaka, Japan) and exposed SK-N-SH cells to this reagent for 2 h prior to exposure to Tm.

Analysis by RT–PCR

Total RNA was isolated from cells transfected with an EBV-based vector (mock, Rz 47, Rz 49 and Rz 68 expression vectors) with Isogen™ (Nippon Gene, Tokyo, Japan), according to the manufacturer's protocol. For confirmation of expression of Rzs, total RNA was reverse transcribed in the presence of Rz down primer (5′-TTCGGCCTTTCGGCCTCATCAG-3′) after incubation with DNase (Roche Diagnostics, Basel, Switzerland). Products were amplified by PCR with Rz up primer (5′-TCCCCGGTTCGAAACCGGGCA-3′) and Rz down primer and reverse transcribed DNA as template, and products of PCR were analyzed by electrophoresis on a 2% agarose gel. We examined the expression of PKR using PKR RT up primer (5′-GGCTGGTGATCTTTCAGCAG-3′) and PKR RT down primer (5′-CCTTCTGGAAATTCTCTTCC-3′) and cDNA as template after reverse transcription in the presence of a poly-dT primer.

Immunocytochemical analysis

We examined the cellular distribution of PKR immunohistochemically as described previously (Bando *et al*, 2000). In brief, SK-N-SH cells were plated on chamber slides and then fixed in PBS that contained 0.1% Triton X-100 and 4% paraformaldehyde. After washing with ice-cold PBS, cells were incubated with normal goat serum for 2 h at room temperature and then with anti-PKR or anti-KDEL antibodies, overnight, at 4°C. Binding of the primary antibody was examined, after reaction with second antibody conjugated with Alexa fluor™ 568 or Alexa fluor™ 488 (Molecular Probes, Oregon), under a confocal laser microscope (LSM510; Carl Zeiss).

Cloning of PKR and generation of alanine-mutated PKR

We amplified the human gene for PKR from SK-N-SH cells using three sets of primers: PKR-F1 f (5′-ATG TCGGACG GCG GCA TGG CTG GTG ATC TTT-3′) and PKR-F1 r (5′-GGA AGG TCA AAT CTG GGT GCC-3′); PKR-F2 f (5′-CAA AAA GAT CTT TGG CAC CC-3′) and PKR-F2 r (5′-GTT ACA AGT CCA AAG TCT CC-3′); PKR-F3 f (5′-GGG GTG GAT TAT ATA CAT TC-3′) and PKR-F3 r (5′-GAG GAT CCC TAA CAT GTG TGT CGT T-3′). Each of the products of PCR was subcloned into pGEM-T (Promega) and its sequence confirmed. A full-length gene for PKR was constructed using the *Bgl*II site in the PKR gene and changing the vector from pGEM-T to pEGFPN3 vector.

Threonine residues 446 and 451 were changed to alanine with a QuickChange™ Site-Directed Mutagenesis Kit (Stratagene, La Jolla, California). To amplify the mutated gene for PKR, we used the following primers: alanine mutant f (5′-GGA AAG GCC AGG AGT AAG GGA GCC TTG CGA TAC-3′) and alanine mutant r (5′-GTA TCG CAA GGC TCC CTT ACT CCT GGC TCG CTT TCC-3′).

Post-mortem specimens and immunohistochemical analysis

Prior to autopsies, we obtained consent from patients and their families to use samples for research only. Some human tissues were obtained from the Brain and Tissue Bank for Developmental Disorders at the University of Maryland (Baltimore, Maryland, USA). Autopsies of AD patients (three; mean age, 71.7 ± 3.3 years) and of age-matched controls who had died of cerebral ischemia or had been clinically and pathologically free of neurological disease (three; mean age, 75.3 ± 4.7 years) were performed between 4 and 8 h after death, and then autopsy specimens were prepared for this study. In each case, diagnosis was confirmed histopathologically. Formalin-fixed samples were used in some experiments.

Preparation of cell extracts and immunoblotting

SK-N-SH cells were collected and lysed in PBS buffer that contained 5 mM EDTA, 1% NP-40, 1 mM DTT (Sigma), 10 μg/ml leupeptin (Roche Diagnostics) and 1 mM Pephabloc SC (Roche Diagnostics). After 5 min on ice, the lysate was centrifuged at 15 000 rpm for 5 min. The supernatant was designated the cytoplasmic fraction. The pelleted nuclei were sonicated in nuclear extraction buffer (20 mM Tris-HCl, pH 7.5, 1% SDS, 5 mM EGTA, 0.5% Triton X-100, 150 mM NaCl, 1 mM DTT, 10 μg/ml leupeptin and 1 mM Pephabloc SC) and the lysate was centrifuged at 15 000 rpm for 5 min. The supernatant was designated the nuclear fraction.

Gray matter was dissected from the temporal cerebral cortex of autopsied brains of four patients with AD and three age-matched controls. Tissues were homogenized in 50 volumes of homogeniza-